

AD-A045 869 COLD REGIONS RESEARCH AND ENGINEERING LAB HANOVER N.H. < F/G 13/1  
EXPERIMENTAL SCALING STUDY OF AN ANNULAR FLOW ICE-WATER HEAT SI--ETC(U)  
JUN 77 J M STUBSTAD, W F QUINN

UNCLASSIFIED

CRREL-77-15

NL

| OF |  
AD  
A045869



END

DATE

FILMED

11-77

DDC

# CRREL

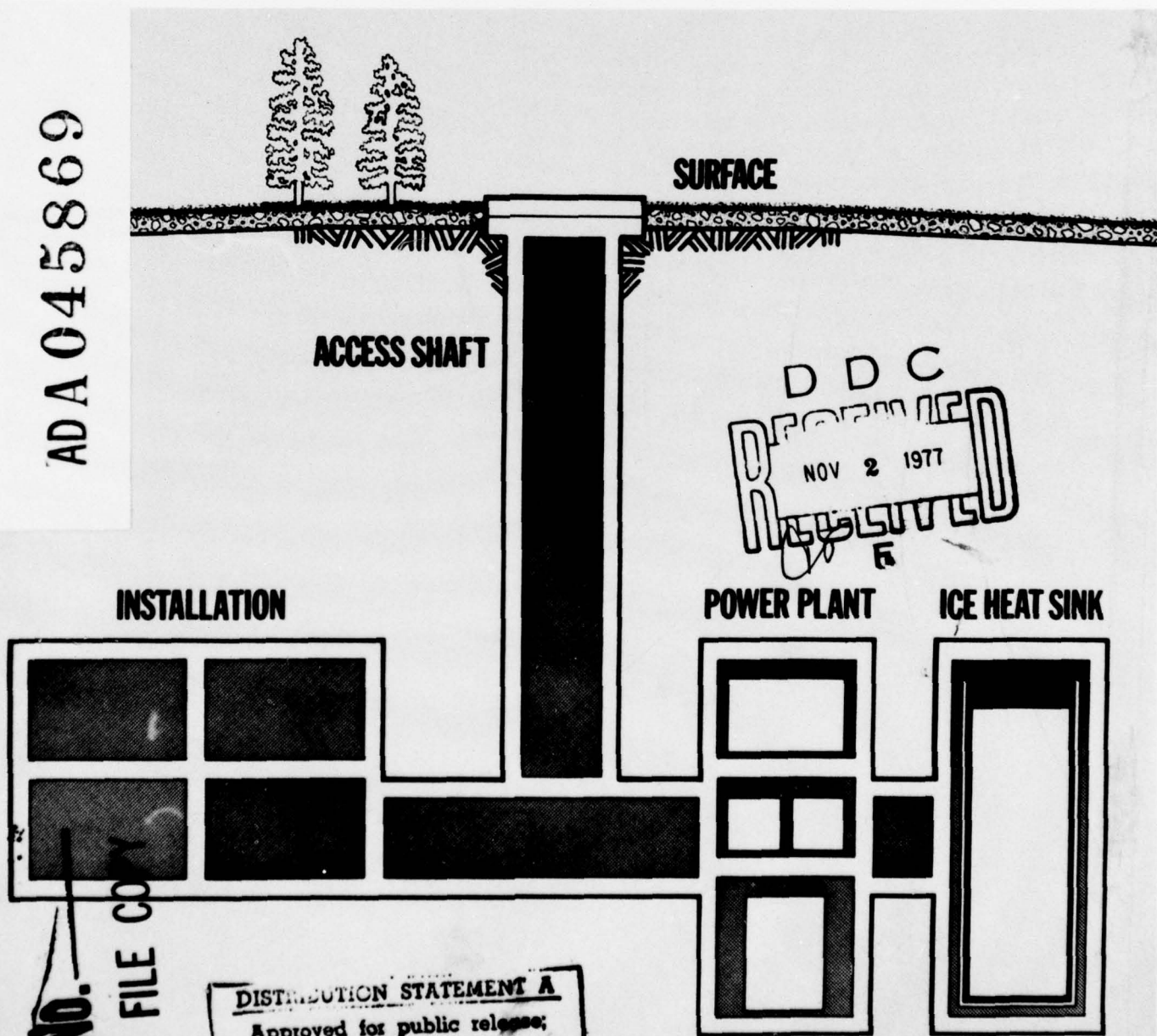
REPORT 77-15

3



## *Experimental scaling study of an annular flow ice-water heat sink*

ADA 045869



No. 120  
DDC FILE COPY

**DISTRIBUTION STATEMENT A**  
Approved for public release:  
Distribution Unlimited

*Cover: Schematic illustration of underground installation with nuclear power plant and ice-water heat sink.*

14 CRREL Report 77-15

6 Experimental scaling study of an annular flow ice-water heat sink,

10 John M. Stubstad and William F. Quinn

11 June 1977

12 6φP.

D D C  
REPRODUCED  
NOV 2 1977  
REPROD  
F

Prepared for  
U.S. ARMY FACILITIES ENGINEERING SUPPORT AGENCY  
By  
CORPS OF ENGINEERS, U.S. ARMY  
**COLD REGIONS RESEARCH AND ENGINEERING LABORATORY**  
HANOVER, NEW HAMPSHIRE

Approved for public release; distribution unlimited.

037 100

mt

Unclassified

SECURITY CLASSIFICATION OF THIS PAGE (When Data Entered)

Unclassified

SECURITY CLASSIFICATION OF THIS PAGE(When Data Entered)

20. (Cont'd).

→ coolant water for approximately one-half its useful life and thereafter behaved like an ordinary stored water reservoir type heat sink. No significant operational problems were discovered. ↑

## PREFACE

This report was prepared by John M. Stubstad, Mechanical Engineer, and William F. Quinn, Chief, Northern Engineering Research Branch, Experimental Engineering Division, U.S. Army Cold Regions Research and Engineering Laboratory. The work was performed for the Facilities Engineering Support Agency (formerly the Engineer Power Group), U.S. Army Corps of Engineers, under Intra-Army Order No. 44018 and 45010 (USA MERDC).

The manuscript of this report was technically reviewed by F.D. Haynes and Dr. Y.C. Yen of CRREL.

The authors are indebted to many people in the CRREL Plant and Equipment Office who assisted in the assembly of the test apparatus. Special mention must be given to E. Lutz, L. Bogie and R. Northam of the Refrigeration Section for their valuable contributions in the installation and insulation of the test model.

The contents of this report are not to be used for advertising or promotional purposes. Citation of brand names does not constitute an official endorsement or approval of the use of such commercial products.

ACCESSION OR	
NTIS	91-16 Section <input checked="" type="checkbox"/>
DC	B-11 Section <input type="checkbox"/>
MANUFACTURED	<input type="checkbox"/>
REPRODUCTION	<input type="checkbox"/>
DISSEMINATION/AVAILABILITY CODES	
SPECIAL	
A	

## CONTENTS

	Page
Abstract .....	i
Preface .....	iii
Nomenclature .....	vi
Conversion factors: U.S. customary to metric units of measurement .....	vii
Introduction .....	1
Description of experiment .....	3
Apparatus .....	3
Test procedure .....	5
Experimental results .....	6
Summary of experimental tests .....	6
Influence of coolant water flow rates .....	8
Approximation of the rate of melting .....	13
Comparison of experimental and computed results .....	16
Comparative analysis of the model sinks .....	18
Approximation of the heat transfer coefficient .....	22
Conclusions and recommendations .....	32
Literature cited .....	34
Appendix A. Experimental data, heat sink Model II .....	35
Appendix B. Heat sink scaling and similarity relationships .....	41
Appendix C. Derivation of the relationships for the heat transfer coefficient, Reynolds and Nusselt numbers .....	45
Appendix D. Determination of freezing rates and refrigeration loads .....	49
Appendix E. Approximation of stresses in the heat sink tank .....	53

## ILLUSTRATIONS

### Figure

1. Model heat sink .....	2
2. Exterior views of the test apparatus .....	2
3. Water level indicating glass and viewport .....	4
4. Inlet header .....	4
5. Thermocouple arrangement .....	4
6. Interior view of the heat sink apparatus .....	4
7. Ice block loading of the Model II sink .....	4
8. Ice melting profiles .....	10
9. Melting of the ice cylinder, 10.00-gpm test .....	10
10. Outlet water temperatures for the Model II tests .....	11
11. Average outlet water temperatures .....	11
12. Flow zones .....	13
13. Melting rates for Model II .....	15
14. Comparison of 2.50-gpm Model II test to 1.00-gpm Model I test .....	20
15. Comparison of 4.73-gpm Model II test to 1.89-gpm Model I test .....	20
16. Comparison of 7.50-gpm Model II test to 3.00-gpm Model I test .....	21
17. Comparison of 10.00-gpm Model II test to 4.00-gpm Model I test .....	22
18. Heat transfer coefficients for Model I, 16,805 Btu/hr tests .....	23
19. Approximated change in radius for Model II tests 1A and 1B .....	26
20. Heat transfer coefficients for Model II .....	28
21. Heat transfer coefficient vs Reynolds number, Model II .....	30
22. Variation in Nusselt number with Reynolds number, Model II .....	30

## TABLES

Table	Page
I. Summary of tests: heat sink Model II .....	7
II. Average heat rejection rates, Model II .....	7
III. Average temperatures during melting .....	12
IV. Melting rates - Model II .....	15
V. Rates of heat rejected to the ice .....	16
VI. Summary of computer predictions .....	16
VII. Average outlet water temperature during melting experimental results and computer predictions .....	17
VIII. Comparison of melting times of experimental and computer models .....	18
IX. Flow rate scaling for Models I and II .....	19
X. Heat transfer coefficients for Model I .....	24
XI. Approximation of the heat transfer coefficient, Model II, test 1B .....	26
XII. Heat transfer coefficient for various Reynolds numbers .....	29

## NOMENCLATURE

<i>Symbol</i>	<i>Definition</i>	<i>Units</i>
<i>A</i>	Area	$\text{ft}^2$
<i>a</i>	Denotes average value	
<i>c<sub>p</sub></i>	Specific heat	$\text{Btu/lbm } ^\circ\text{F}$
<i>d</i>	Thickness	in.
<i>D</i>	Diameter	ft
<i>DE</i>	Equivalent diameter	ft
<i>E</i>	Young's modulus	$\text{lbf/in.}^2$
<i>f</i>	Subscript referring to final value	
<i>Gr</i>	Grashof number	
<i>h</i>	Heat transfer coefficient	$\text{Btu/hr ft}^2 \ ^\circ\text{F}$
<i>H</i>	Height	ft
<i>i</i>	Subscript referring to ice	
<i>k</i>	Thermal conductivity	$\text{Btu/hr ft } ^\circ\text{F}$
<i>L</i>	Latent heat of fusion	$\text{Btu/lbm}$
<i>m</i>	Subscript referring to melting	
<i>M</i>	Mass	$\text{lbm}$
<i>N<sub>s</sub></i>	Heat storage parameter	
<i>Nu</i>	Nusselt number	
<i>o</i>	Subscript referring to initial value	
<i>Pr</i>	Prandtl number	
<i>Q</i>	Heat	$\text{Btu}$
<i>Q̇</i>	Rate of heat transfer	$\text{Btu/hr}$
<i>R</i>	Radius	ft
<i>Re</i>	Reynolds number	
<i>s</i>	Subscript referring to sink	
<i>t</i>	Time	hr
<i>T</i>	Temperature	$^\circ\text{F}$
<i>U</i>	Mean flow velocity	ft/hr
<i>V</i>	Volume	$\text{ft}^3$
<i>w</i>	Subscript referring to water	
<i>W</i>	Mass flow rate	$\text{lbm/hr}$
<i>α</i>	Rate of change of temperature	$^\circ\text{F/hr}$
<i>ε</i>	Strain	in./in.
<i>σ</i>	Stress	$\text{lbf/in.}^2$
<i>ρ</i>	Density	$\text{lbm/ft}^3$
<i>θ</i>	Dimensionless time	
<i>v</i>	Kinematic viscosity	$\text{ft}^2/\text{hr}$

## CONVERSION FACTORS: U.S. CUSTOMARY TO METRIC (SI) UNITS OF MEASUREMENT

These conversion factors include all the significant digits given in the conversion tables in the *ASTM Metric Practice Guide* (E 380), which has been approved by the Department of Defense. Converted values should be rounded to have the same precision as the original (see E 380).

<i>Multiply</i>	<i>By</i>	<i>To obtain</i>
inch	25.4*	millimeter
foot	3.048*	meter
gallon/minute	$6.309020 \times 10^{-5}$	meter <sup>3</sup> /second
pound-mass	0.4535924	kilogram
pound-mass/foot <sup>3</sup>	16.01846	kilogram/meter <sup>3</sup>
pound-mass/hour	$1.259938 \times 10^{-4}$	kilogram/second
pound-force/inch <sup>2</sup>	6.894757	kilopascal
Btu/hour	0.2928751	watt
Btu/pound-mass °F	4184.000	joule/kilogram kelvin
Btu/hour foot <sup>2</sup> °F	5.674466	watt/meter <sup>2</sup> kelvin
degree Fahrenheit	$t_{\circ C} = (t_{\circ F} - 32)/1.8$	degree Celsius

\* Exact.

## EXPERIMENTAL SCALING STUDY OF AN ANNULAR FLOW ICE-WATER HEAT SINK

J. Stubstad and W. Quinn

### INTRODUCTION

The investigation of efficient methods of storing the waste heat produced by the generation of power in hardened underground installations has resulted in the development of several new concepts for short-term heat sinks. Some of the methods explored include the use of favorable in-situ conditions to provide the necessary heat storage capacity.<sup>5 9 12 13 17</sup> For example, in one method, steam from the turbine is condensed on the surfaces of rock tunnels or passageways. The waste heat is thus "stored" in the rock media surrounding the tunnel.<sup>9 12 13</sup>

Another concept involves the use of an ice-water heat sink which is relatively independent of in-situ ground conditions (see cover). Waste heat is stored by the conversion of ice to water and subsequent heating of the water. Relative to other types of liquid reservoir heat sinks, the ice-water sink provides a longer period of low and essentially constant temperature coolant water for the condenser. This results in high overall thermal efficiencies for the power plant, particularly during the more critical early stages of sink usage. In addition, the large amount of heat required to convert ice to water results in high volumetric efficiency. This increased storage of heat per unit volume of sink reduces construction costs.

Using a 4-ft-diam and 6-ft-high scale model, CRREL initially examined the feasibility and practicality of the ice-water concept.<sup>3</sup> A computer program was developed during this initial study to numerically simulate the temperature-time history of the model sink. This study concluded that an annular flow ice-water heat sink was feasible and that the computer program

could predict the behavior of the scale model with a reasonable degree of accuracy. A subsequent study was conducted, using the same model but examining different ice forms, specifically ice cylinders, ice blocks and ice cubes.<sup>14</sup> It concluded that the use of a solid ice cylinder represented the best overall balance between a desired low, essentially constant outlet water temperature and optimum heat storage capacity.

A major concern recognized during these initial studies was the potential problem in scaling the results of this rather small model to a large prototype. With respect to the 4-ft-diam by 6-ft-high model, a prototype sink (estimated to be on the order of 65 ft in diameter and 110 ft high) would be almost 5000 times larger on a volumetric basis. With scaling factors of this magnitude it was quite possible that undesirable characteristics in the prototype might not be observable in the scale model. As a result another test program was sponsored by the Engineer Power Group (now Facilities Engineering Support Agency) to investigate possible scaling effects. Space limitations within the CRREL facility restricted the overall size of the new model (Model II) to 6 ft in diameter by 10 ft high, yet this resulted in a volumetric increase of 375% over the previous model. The volumetric ratio between a prototype sink and the new Model II apparatus is 1300 to 1.

In addition to testing scaling effects, the Model II test series also investigated some of the practical operational problems that had been encountered during previous test programs, for example, corrosion protection, economical methods of creating the ice cylinder, the point of introduction effect of inlet

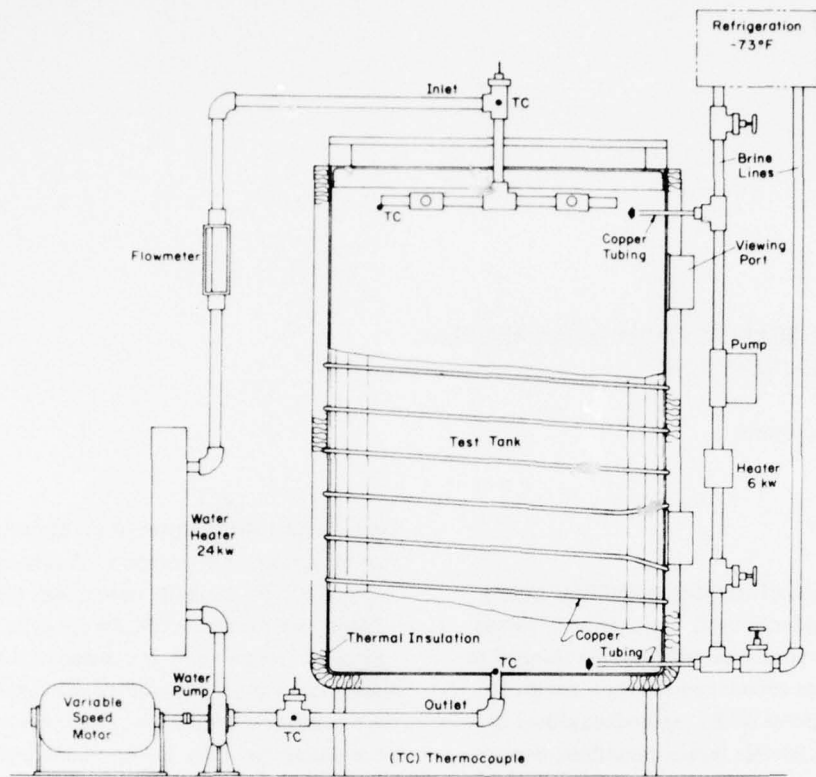
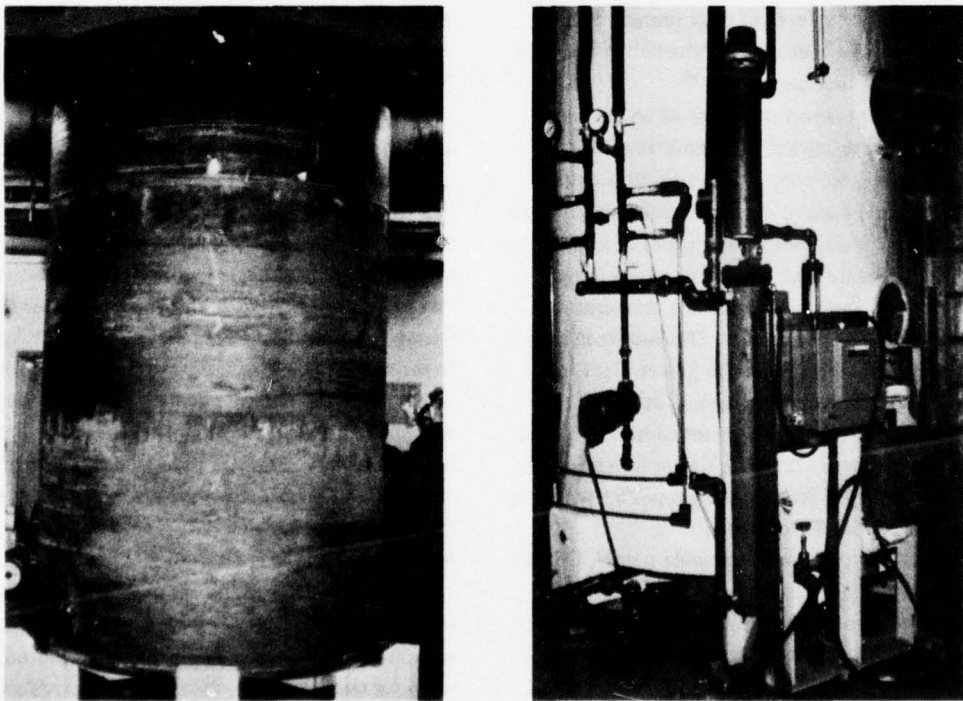


Figure 1. Model heat sink.



a. Prior to insulation.

b. Completed.

Figure 2. Exterior views of the test apparatus.

water on the melting geometry, and efficient methods of melting the initial annulus. Although none of the problems encountered were of the type that would make the heat sink concept infeasible, they could be particularly bothersome in an installation the size of a prototype sink.

This report represents: 1) the experimental results using the larger Model II test apparatus, 2) a comparison of the test results with those predicted by the previously developed computer program, and 3) a comparison of the results with tests conducted in earlier programs.

## DESCRIPTION OF EXPERIMENT

### Apparatus

The Model II experimental apparatus is illustrated in Figures 1 and 2. It represents an enlarged version of the model used in the previous studies. Due to restrictions in laboratory overhead room, the height of the new model (Model II) was limited to 10 ft; a nominal diameter of 6 ft was selected to provide a length/diameter ratio similar to that of a prototype sink 110 ft high and 65 ft in diameter. Volumetrically the new test apparatus was 3½ times larger than the previously used 6-ft-high, 4-ft-diam model (Model I).

To freeze the water in the tank, a trichloroethylene brine at a nominal -73°F temperature was circulated through 500 ft of ¼-in.-diam copper tubing wrapped around the sides and bottom of the tank. The tank walls were insulated with 3-in. high-density blanket-type Fiberglas insulation and covered with a PVC vapor barrier. Two layers of 2-in. sheets of polyurethane were used to insulate the bottom, and a paint-on vapor barrier was used to seal the bottom and corners. The cover, a composite of 2x4's and ½-in. plywood, was insulated with inlays of 2-in. polyurethane. The insulation provided an excellent barrier to environmental influences, yielding an overall heat transfer coefficient of only 0.18 to 0.20 Btu/hr ft<sup>2</sup> °F between the outside and inside surfaces. The heat transfer coefficient for the insulated apparatus was determined by filling the tank with hot water and monitoring the decrease in bulk water temperature during a 24-hr period. Combined with air temperature readings during this period, the decrease in sensible heat was converted into a mean heat transfer coefficient.

To prevent possible development of the high stresses associated with the entrapment of liquid water by forming ice, a system was installed to bubble air through the center of the tank and across the surfaces of the viewports. The air stream provided a continuous free path to the surface and thereby prevented the entrapment of liquid water by the ice.

During the previous model tests difficulties were experienced in providing corrosion protection, due to the extreme variations in tank wall temperature of -70°F to +120°F. Large stresses produced by the different coefficients of thermal expansion for the surface coating and the steel wall resulted in the separation of the finish from the wall and the loss of corrosion protection. Discussions with manufacturers of various corrosion-resistant paints indicated that no standard paint was manufactured which could withstand both the extreme low and high temperatures and high humidity conditions of the model sink. The solution was found through the application of a cold galvanizing compound to the interior surfaces. This product, manufactured by the ZRC Corporation, is a mixture of approximately 95% zinc and 5% binder, which provides a surface finish having the same basic characteristics as hot dip galvanizing. In the six experimental tests conducted during the Model II program, the only failures of this coating occurred in areas where the steel surface had not been sufficiently cleaned prior to coating. A coating of this type would be recommended for a prototype steel tank.

As with the Model I apparatus, two viewports were installed in the tank wall. Observations of the melting geometry were made by using the viewports and an access opening in the tank cover. A probe assembly, inserted through the cover, measured the changing shape of the ice cylinder during a test. The probe consisted of a stainless steel rod and a mounting block to locate it on the cover; the rod was lowered into the tank until it touched the ice cylinder. By measuring the depth of the ice from the tank cover, the height of the ice at that point was determined. The probe was then moved outward along one of the three radial slots in the cover. One slot was located directly above one of the water inlet pipes to permit examination of the scouring pattern. The two other slots were located on a common diameter but between two outlet pipes to avoid as much of the scouring influence as possible.

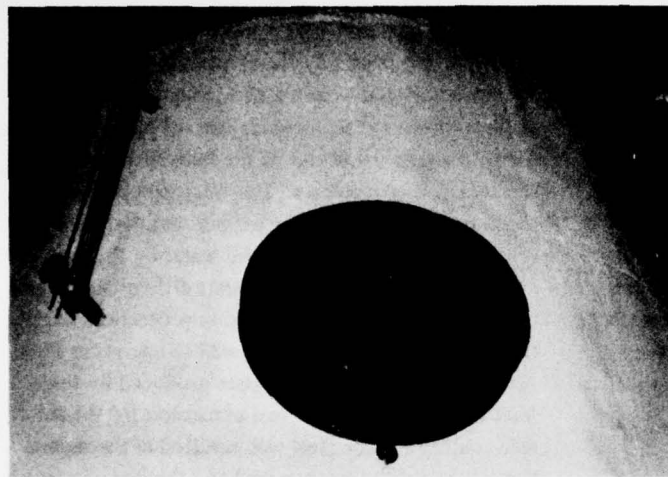


Figure 3. Water level indicating glass and viewport (covered).

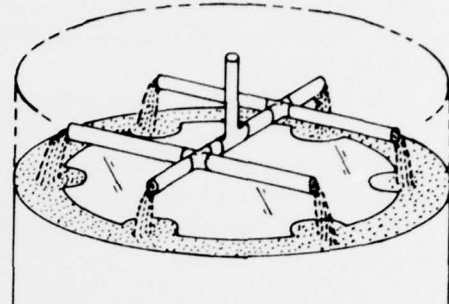


Figure 4. Inlet header.

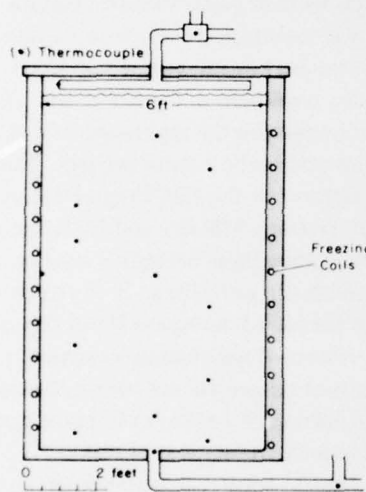


Figure 5. Thermocouple arrangement.

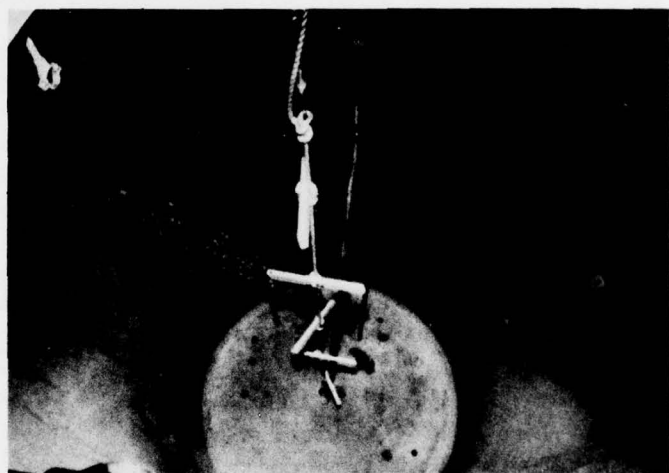


Figure 6. Interior view of the heat sink apparatus.

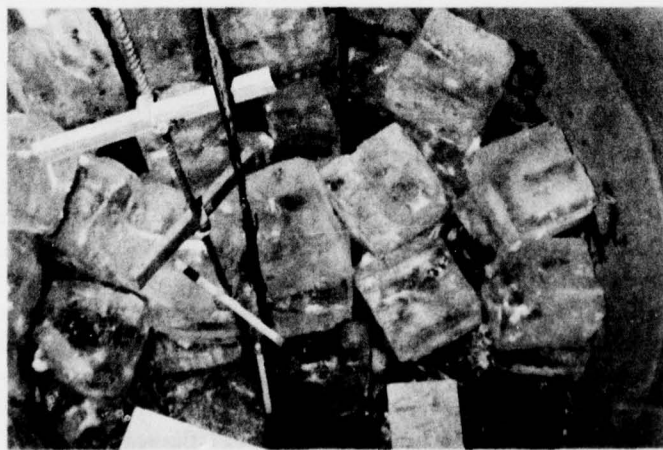


Figure 7. Ice block loading of the Model II sink.

Changes in water level were monitored using a water level indicating tube (Fig. 3). These changes were then related to the volumetric contraction associated with conversion of the relatively low density ice to water, as an indication of the gross melting rate.

To permit comparison with the Model I test series, a central coolant water outlet and a six-point inlet header were again used in this series (Fig. 4). Although more efficient methods of introduction and removal of the coolant water had been proposed, it was desired to replicate the previous test conditions as much as possible.

Temperature variations within the sink were measured by using three strings of thermocouples, one placed along the vertical centerline, and the others along vertical lines at the  $\frac{1}{2}$  and  $\frac{3}{4}$  radial position (Fig. 5). The thermocouples were fixed in position by attaching them to ropes tied to anchor points at the top and bottom of the tank. The thermocouples were monitored with a Leeds and Northrup chart recorder, with an extra thermocouple in an ice bath for calibration purposes. Inlet and outlet water temperatures were measured using thermocouples, two in the inlet header and two in the outlet pipe; a Kaye data logger was used to take readings at 20-min intervals.

A 24-kW immersion heater was used to simulate the power plant condenser; control of the rate of heating was provided by a Variac transformer. A  $\frac{1}{2}$ -hp variable-speed DC motor with a rotary displacement pump was used to circulate water through the heater and back into the sink. Flow rates were monitored with either a 0.5 to 6.0 gpm or 1.72 to 17.2 gpm rotameter, the latter being used only when test flow rates exceeded 5.0 gpm. The heater and pump module is illustrated in Figure 2b.

Once the sink had been completely frozen, an initial annulus was created by circulating hot brine through the refrigeration tubing. A 6-kW immersion heater was used to heat the brine.

The use of hot brine, rather than electric heating tapes which were employed with the previous apparatus, was chosen because this type of system provides maximum utilization of the refrigeration lines and is believed to better simulate probable heating and cooling schemes for a prototype sink.

During a test, motion of the ice cylinder was prevented by an anchor system consisting of several boards fastened to a rope positioned along the vertical centerline of the tank. While some rotational mo-

tion from uneven melting did occur, the gross overall movement was insignificant. The ice anchor system and thermocouples are shown in Figure 6.

#### Test procedure

Two techniques were employed to form the ice cylinder. The primary method involved filling the test tank with water and freezing inward from the tank wall. Approximately six days were required to completely freeze all the water. Two tests were conducted with a second method, the loading of a mixture of ice and water prior to the start of freezing. These tests, employing an initial ice load of 6000 to 8000 lb in 50-lb blocks and a water load of 6000 to 8000 lb, reduced the freezing period to about five days. A view of the heat sink during the block loading operation is shown in Figure 7. The cost effectiveness of this procedure is somewhat obscured by the availability of a large capacity on-line refrigeration system at CRREL, but even an initial starting mass of 50% ice does not significantly affect the freezing period. An explanation is that the longest part of the freezing period is associated with freezing the center of the ice cylinder, and an initial load of ice does not increase the rate of heat conduction through the ice. Of course this procedure does result in a substantial decrease in the on-site refrigeration load. (The possibility of generating higher packing ratios, i.e. initial ice to total mass ratios, was investigated in a previous study,<sup>14</sup> and it was concluded that for common ice shapes, such as cubes or blocks, a maximum of about 61% ice was the best that could be obtained.) A detailed analysis of the freezing process is given in Appendix D.

Once freezing had been completed, the sink was allowed to stand at room temperature for a period of one to two days. A temperature gradient of  $-70^{\circ}\text{F}$  at the tank wall to  $32^{\circ}\text{F}$  at the center of the tank normally existed at the moment when complete freezing had occurred; this standby period allowed temperature equilibration to occur. When the tank wall had reached a temperature of approximately  $-10^{\circ}\text{F}$ , the brine heater was activated and the melting of an initial annulus commenced. Since the hot brine flowed around the tank through one continuous loop, it was necessary to reverse the direction of brine flow several times in order to melt a uniform annulus. This technique was only partially successful; the initial annulus normally varied from 1 to 2 in. at the top

to  $\frac{1}{2}$  to  $\frac{1}{4}$  in. at the bottom corner. In future experiments the brine system should be composed of several circuits connected in a parallel manner to ensure development of a more uniform annulus.

After the initial annulus had been formed and the average ice temperature was between  $28^{\circ}$  and  $32^{\circ}$ F, water was added to completely submerge the ice cylinder. By covering the ice block with water during the test, changes in the water level could be related to the amount of ice melted at any time. After a short period of time to allow this added water to reach an equilibrium temperature, the test was begun.

During the test the coolant water flow rate and the temperature difference between the sink inlet and outlet water were monitored to check the rate of heat rejection. Readings of the change in water level and shape of the ice were taken at random intervals. Once the ice was completely melted and the outlet water temperature was at least  $60^{\circ}$ F, the test was stopped and a measurement was made of the bulk water temperature. From this and the initial ice mass and temperature, a heat balance was computed as a check on the nominal heat rejection rate.

## EXPERIMENTAL RESULTS

### Summary of experimental tests

Six experimental tests were conducted with a nominal heat rejection rate of 42,013 Btu/hr. Coolant water flow rates varied from 2.50 to 13.50 gpm. Both the heat rejection rate and coolant water flow rates were selected by using the scaling relationships developed by Brown and Quinn.<sup>3</sup> Table I summarizes the tests.

By measurement of the ice cylinder at the start of a test and the total change in sink volume at the completion of melting, the initial ice mass was determined. In the six tests the initial ice mass varied from a low of 12,250 lbm in test 2 to a high of 13,420 lbm in test 5, the ice mass averaging 12,970 lbm. The total mass (both liquid and solid states) contained in each test varied from 14,150 lbm in test 4 to 14,370 lbm in test 3, with an average of 14,280 lbm. Of critical importance to the volumetric efficiency of an ice-water heat sink is the percentage of total mass in the form of ice; in this test series it was found that the ratio varied from a low of 85.7% to a high of 94.0% with an average load factor of 90.8%.

Three separate procedures were employed for comparison to establish the average heat rejection rate during the tests.

*Procedure 1.* With the heat sink inlet and outlet coolant water temperatures and the flow rate known at any particular instant, the heat rejection rate  $\dot{Q}$  can be determined from

$$\dot{Q} = Wc_{pw}(T_{in} - T_{out}) \quad (\text{Btu/hr})$$

where  $W$  = mass flow rate (lbm/hr)

$c_{pw}$  = specific heat of water (Btu/lbm  $^{\circ}$ F)

$T_{in}$  = inlet temperature ( $^{\circ}$ F)

$T_{out}$  = outlet temperature ( $^{\circ}$ F).

To determine the average value of the heat rejection rate  $\dot{Q}_a$  during the test, the following formula can be used for "n" time intervals:

$$\dot{Q}_a = \frac{1}{n} \sum_1^n \dot{Q} = \frac{1}{n} Wc_{pw} \sum_1^n (T_{in} - T_{out}) \quad (1)$$

where the mass flow rate  $W$  and specific heat  $c_p$  have been assumed to be constant. In practice, readings were taken at 20-min intervals so that the average value is based on 150 to 200 separate temperature readings.

*Procedure 2.* At the completion of a test a heat balance was conducted to examine the reliability of the previous method. In this method three heat storage components must be considered: sensible heating of the ice  $Q_i$ , latent heat  $Q_m$ , and sensible heating of the water  $Q_w$ . The initial ice temperature was estimated by averaging readings from the thermocouples in the ice (12 thermocouples in all) and assuming that this average value was the mean initial ice temperature  $T_i$ . Thus the sensible heat storage capacity of the ice is

$$Q_i = M_i c_{pi} (32 - T_i) \quad (2a)$$

where  $M_i$  is the initial ice mass (lbm), and  $c_{pi}$  is the specific heat of ice (Btu/lbm  $^{\circ}$ F). The latent heat storage capacity for the melted ice is

$$Q_m = L M_i \quad (2b)$$

where  $L$  is the latent heat of fusion (144 Btu/lbm). Finally the sensible heat storage capacity of the water is

Table I. Summary of tests: heat sink Model II.

Tank size: 6 ft diam, 10 ft high;  
Nominal heat rejection rate: 42,013 Btu/hr.

Test no.	Nominal flow rate (gpm)	Initial ice mass (lbm)	Total mass ice & water (lbm)	Ratio ice/total mass (%)
1A	4.73	13,210	14,300	92.4
1B	4.73	13,290	14,300	92.9
2	2.50	12,250	14,300	85.7
3	10.00	12,750	14,370	88.7
4	7.50	12,900	14,150	91.2
5	13.50	13,420	14,270	94.0
Average values		12,970	14,280	90.8

Table II. Average heat rejection rates, Model II.

Nominal heat rejection rate: 42,013 Btu/hr.

Test no.	Nominal flow rate (rpm)	$\dot{Q}$ Procedure 1 (Btu/hr)	$\dot{Q}$ Procedure 2 (Btu/hr)	$\dot{Q}$ Procedure 3 (Btu/hr)
1A	4.73	41,305	38,570	38,600
1B	4.73	40,150	35,050	39,340
2	2.50	41,140	40,720	29,060*
3	10.00	41,410	38,530	36,240
4	7.50	42,090	35,920	38,090
5	13.50	40,260	†	34,790
Average		41,060	37,760	37,410*
Deviation from nominal rate		-2.3%	-10.1%	-11.0%

\* Value of test 2 not included in average (see text).

† Not available; test ended prematurely due to equipment failure.

$$Q_w = M_i c_{pw} (T_f - 32) + M_w c_{pw} (T_f - T_0) \quad (2c)$$

where  $T_f$  = final water temperature at the end of the test ( $^{\circ}$ F)

$T_0$  = initial water temperature ( $^{\circ}$ F)

$M_w$  = mass of water in the annulus at the start of the test at an initial temperature of  $T_0$  (lbm).

The average heat rejection rate by the heat balance method is determined from

$$\dot{Q}_a = \frac{Q_i + Q_m + Q_w}{t_f} \quad (2d)$$

where  $t_f$  = time to reach final water temperature  $T_f$  (hr).

**Procedure 3.** This method considered the sensible heating of the water within the sink after all ice was completely melted. It is assumed that the rate of

temperature change of the entire sink was the same as the rate of change of the outlet coolant water; that is

$$\frac{dT_b}{dt} \approx \frac{dT_{out}}{dt}$$

where  $T_b$  is the bulk "mixing cup" temperature of the sink.

Such an assumption represents a good approximation only when there is a high degree of mixing within the sink and is not valid when density-induced stratification occurs. A least squares fit is made to the outlet water temperature curve. The slope of this line is  $dT_{out}/dt$  so that the straight line heat rejection rate  $\dot{Q}_a$  is

$$\dot{Q}_a = M_s c_{pw} \frac{dT_{out}}{dt} \quad (3)$$

where  $M_s$  is the total mass of water contained within the sink.

The values of the average heat rejection rate using these three methods have been tabulated in Table II with the overall average for all tests combined. As noted, the third method cannot be used when density-related stratification effects predominate, such as in test 2. For this test a heat rejection rate based on the slope of the outlet water temperature curve is meaningless and has not been included in the overall average.

A close correlation exists between the overall average values derived by Procedures 2 and 3. It is felt that the actual experimental heat rejection rates lie between the maximum and minimum limits established by these three methods. Thus the experimental heat rejection rates were between 2 and 11% less than the nominal value of 42,013 Btu/hr.

In the three procedures used to calculate the average heat rejection rate, heat transfer to the surroundings was assumed to be negligible and was not included. The validity of this assumption can be shown by examining the results of test 3. During this test the average air temperature was 63.3°F. A thermocouple mounted on the inside tank wall at one-half its height indicated an average tank wall temperature of 53.8°F for the test. Assuming that this temperature is indicative of the mean tank wall temperature, the resulting average temperature difference of 9.5°F across the tank insulation results in a heat gain of only 500 Btu/hr. Such a rate is approximately 1% of the nominal applied heat load and therefore is insignificant in comparison to the applied heating rate.

#### Influence of coolant water flow rates

Over the range of flow rates tested it was found that a well-defined transition occurs in the pattern of water flow through the sink. At the lowest flow rates distinct water layers were formed, resulting from differences in density of the inlet water and the water within the sink. The warmer inlet water formed a layer on top of the colder water within the sink, with a rather distinct boundary between them. This boundary proceeded very slowly down the tank and produced an almost top-to-bottom melting pattern. This pattern, illustrated in Figure 8a, shows the ice profile for test 2 conducted at a coolant water flow rate of 2.50 gpm. It should be noted that the horizontal upper ice surface indicates an almost constant rate of melting across the entire upper

surface, even though the heated inlet water was introduced at the two-thirds radial position.

This phenomenon is also apparent after all the ice has melted, as can be seen in the time-temperature history of the outlet water temperature (Appendix Figure A2). Note that when melting is completed the outlet water temperature rapidly increases and then stabilizes at a constant temperature which equals that of the inlet water prior to the sudden increase. It then remains at this temperature for approximately 10 hours when it again shows a sharp increase. By assuming a uniform velocity profile, the flow rate of 2.50 gpm through a 6-ft-diam cylinder would result in a net downward velocity of 0.142 in./min. Under conditions where there is absolutely no mixing between layers, approximately 11.5 hours would be required for this theoretical layer to traverse the 98 in. from the water surface to the outlet. The actual period of this temperature plateau was 10.5 hours. With a modest allowance for some mixing of the water along the boundary, which would reduce the time required for the hotter inlet water to influence the outlet water temperature, it is found that the experimental results agree rather well with such a flow process.

Thus, at low flow rates during this post-melting stable temperature period, the outlet water temperature is essentially unaffected by the addition of heated inlet water; that is, the outlet water temperature will be the same whether the condenser water is returned to the sink or wasted. The duration of this plateau period can be expressed simply as

$$t = 0.9 \frac{M_s}{W} \text{ (hr)} \quad (4)$$

where  $W$  is the mass flow rate of water in lbm/hr. The factor of 0.9 is used to account for mixing effects at the boundary.

It should be emphasized that this formula applies only to low coolant water flow rates, 2.5 gpm and less in the Model II sink, and only under conditions of constant coolant flow and heat rejection rates.

If we attempt to apply the same approach to the tests having a flow rate of 4.73 gpm, the formula predicts that for the nominal heat rejection rate of 42,013 Btu/hr there should be a post-melting stable temperature period lasting 5.5 hours. A temperature plateau of this type did not occur; instead, changes of slope in the outlet water temperature-time curve

developed at five- to six-hour intervals, indicating that there was some tendency for stratification (Fig. A1). These periods also indicate a mixing of warmer inlet water with the cooler sink water. It would appear that density-induced stratification is not the dominant flow process through the sink at this flow rate, but rather there is probably an almost equal balance between overall mixing and stratification. Thus the evidence of thermal stratification prevalent in the 2.50 gpm test is sharply reduced at higher flow rates, and the transition from stratified to mixed flow occurs in the neighborhood of 4.73 gpm for the Model II apparatus.

Following the same reasoning it would be expected that the increase in flow rate from 4.73 to 7.50 gpm would result in the total disappearance of density-related effects, with mixed flow being the dominant mode. As shown in Appendix Figure A3 the outlet water temperature curve for the 7.50-gpm test does become a straight line after completion of melting, the increasing linearity resulting from the mixing of warmer inlet water with the colder water within the sink. (The terms *warmer* and *colder* are relative, since in this test there is only an 11°F difference in temperature between the outlet and inlet water.)

This behavior is also apparent at the two highest flow rates used: 10.00 and 13.50 gpm. For flow rates greater than 7.50 gpm in the Model II apparatus, the sink exhibits a mixed flow condition after completion of melting. As in the low flow rate tests, this leads to a rather simple formula for predicting the post-melting temperature-time behavior — the heating of a well-mixed large mass of water. In parametric form this is expressed by

$$T_{\text{out}}(t) = \alpha(t-t_m) + T_m \quad (^\circ\text{F}) \quad (5a)$$

where  $t$  = running time variable (hr)

$t_m$  = time at which melting was completed

$T_m$  = outlet water temperature at the completion of melting (°F)

$\alpha$  = the rate of temperature change of the sink water (°F/hr)

where

$$\alpha = \frac{\dot{Q}}{M_s c_p} \quad (5b)$$

This equation may be used for either a constant or variable rate of heat rejection; however, in the latter case  $\alpha$  will also become a variable and the graph of the outlet temperature will be a curved rather than straight line.

As stated previously, further increases in flow rate (i.e. to 10.00 and 13.50 gpm) did not result in any changes in the shape of the outlet water temperature curve but only affected the mean outlet water temperature.

In conjunction with the change from stratified to mixed flow at 4.73 gpm there was also a significant change in the melting pattern. In the 2.50-gpm flow rate test, ice melting proceeded vertically from the top downward with a uniform rate of melting across the top. The melting pattern for the 10.00-gpm test was predominantly radial. As might be anticipated from the stratified and mixed flow conditions which developed, the melting geometry of the 4.73-gpm test shows both vertical and radial melting patterns. This would indicate that stratified flow produces a vertical melting (top-downward) pattern, whereas mixed flow produces radial melting.

These flow rate effects can also be illustrated by examining the melting pattern of the ice directly beneath one of the inlet pipes (Fig. 8). In all tests the ice was completely submerged. In the 2.50-gpm test the inlet water tends to create a smooth surface. This indicates that the inlet water does not come in direct contact with the ice, except during the first few hours, but is separated from it by the water above the ice surface. This is not true for the 4.73-gpm flow rate, as shown in Figure 8b. From the start of the test the inlet water produces a high rate of melting near the inlet, as evidenced by the ice scour pattern. This effect has a decreasing influence; by the twenty-second hour the melting pattern begins to resemble the geometry of the 2.50-gpm test. The scouring effect becomes increasingly important as flow rate is increased, so that for the 10.00-gpm test, shown in Figure 8c, it predominates. After just eight hours, melting is almost completely radial with very little change in the ice height. This cutting effect of the inlet water is well illustrated in Figure 9, which shows the ice surface during the 10.00-gpm test. Note the almost vertical slice in the ice surface in the vicinity of the inlet. This indicates that at this flow rate the inlet water causes melting along a significant length of the ice cylinder.

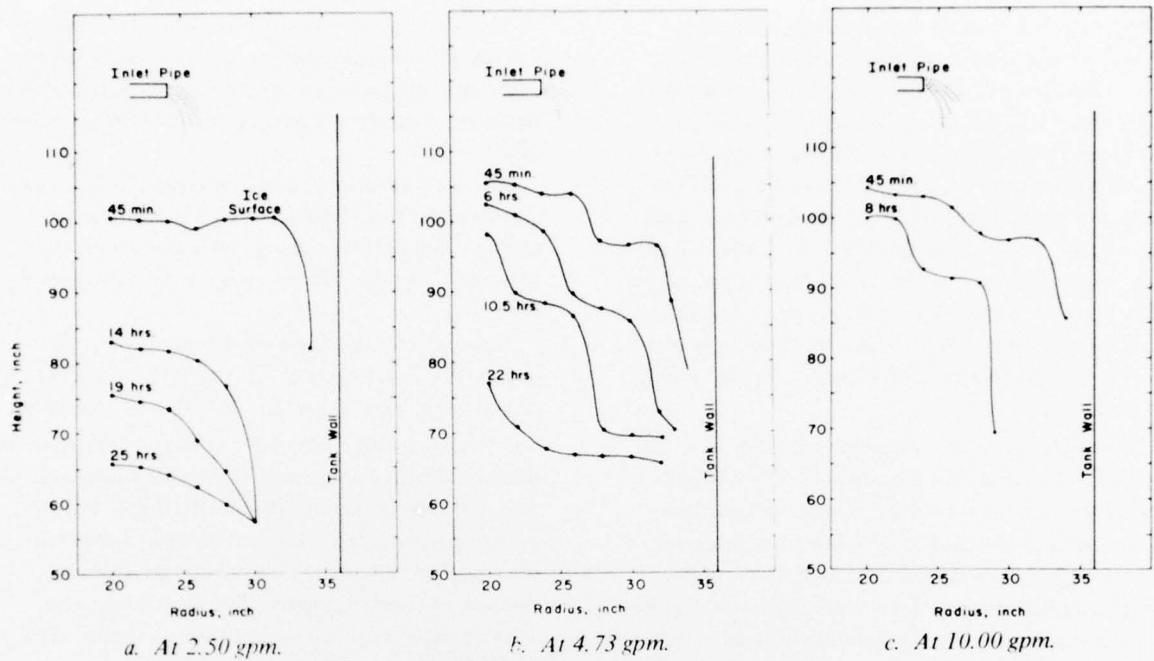


Figure 8. Ice melting profiles.

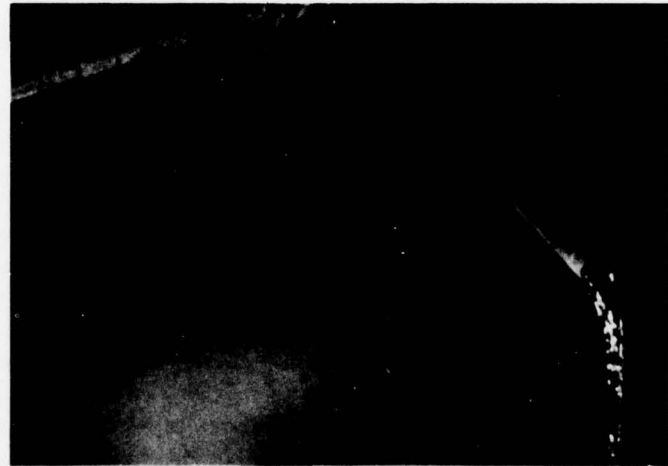


Figure 9. Melting of the ice cylinder, 10.00-gpm test.

Another means to investigate the influence of the coolant water flow rate is to compare outlet temperature-time histories for the tests, as shown in Figure 10. During the melting stage the test results may be partitioned into two general categories: one for the 10.00- and 13.50-gpm tests and the other for the 2.50-, 4.73- and 7.50-gpm tests. For the two higher flow rate tests, there is a rather smooth rate of change in outlet water temperature starting at about

41°F and linearly increasing at a constant rate of approximately  $1/8$  degree/hr. For the three low flow rate tests, there are fluctuations in the outlet water temperature on the order of 1 to 3 degrees Fahrenheit within an overall operating range of 36° to 40°F. Since the maximum density of water occurs at 39.2°F, it is possible that these observed fluctuations are the result of an unstable flow condition due to density inversion effects. This would indicate that, up to 7.5-gpm

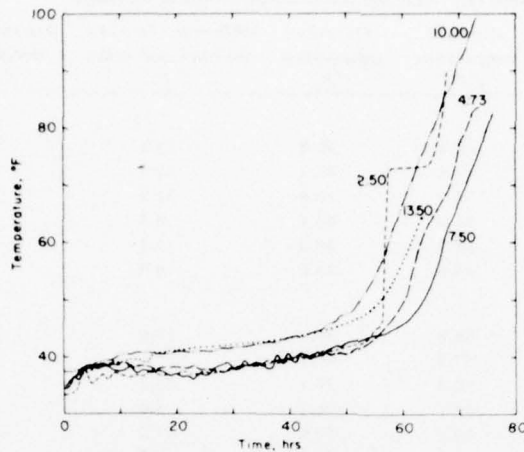


Figure 10. Outlet water temperatures for the Model II tests.

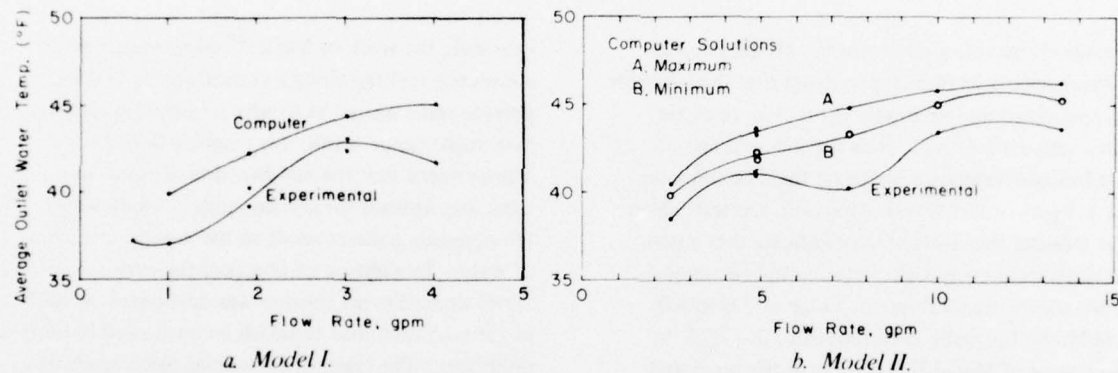


Figure 11. Average outlet water temperatures.

flow rates, the outlet water is influenced by density inversion, the effects of which are apparently insignificant at the higher flow rates.

The average outlet water temperature for the entire melting period vs the nominal water flow rate has been plotted in Figure 11a and tabulated in Table III. It can be seen that except for the 7.50-gpm test the average outlet water temperature lies along a rather smooth curve which reaches a maximum value of 43.5°F for flow rates of about 10.00 gpm and higher. The dip which occurs at 7.50 gpm could have resulted from either density-related effects or from a low heat rejection rate during the test. While the possible occurrence of a low heat rejection rate is not indicated in Table II, the observed changes in water level during the melting period indicate that this was a distinct possibility (see Fig. 13). A reduction in the heat load would naturally

result in a lower outlet water temperature; however, the significantly lower average outlet water temperature at this flow rate was quite probably influenced more by density-related effects. The possible occurrence of a low heat rejection rate and its influence are discussed in later sections.

Average outlet water temperatures during the melting period vs coolant water flow rates for the Model I study are shown in Figure 11b. These results indicate that a maximum average outlet water temperature condition developed at the intermediate flow rates. In contrast the results of the Model II study indicate a minimum temperature at an intermediate flow rate. The existence of a maximum in one study and a minimum in the other could be the result of the scaling relationships employed to relate the models. The scaling procedure used postulates a proportional relationship between the

**Table III. Average temperatures during melting.**

Test no.	Flow rate (gpm)	Avg inlet temperature (°F)	Avg outlet temperature (°F)	Difference between avg inlet and outlet (°F)	Avg bulk water temperature (°F)*
<b>Model II</b>					
1A	4.73	58.4	40.8	17.5	49.6
1B	4.73	58.5	41.2	17.3	49.9
2	2.50	71.9	38.5	32.9	55.2
3	10.00	51.7	43.4	8.3	47.6
4	7.50	51.7	40.3	11.2	46.0
5	13.50	49.6	43.6	6.0	46.6
<b>Model I</b>					
1S <sub>1</sub>	1.89	56.8	39.2	17.6	48.0
1S <sub>2</sub>	1.89	57.9	40.1	17.8	49.0
2S	1.00	70.3	37.1	33.3	53.7
3S	4.00	49.1	41.7	8.6	45.4
4S <sub>1</sub>	3.00	54.2	43.0	11.2	48.6
4S <sub>2</sub>	3.00	53.4	42.3	11.2	47.9
5S	0.62	101.7	37.2	64.6	69.5

\* Average bulk water temperature =  $1/2(T_{in} + T_{out})$ .

flow rates of the two models; for the Model I and II tests these scaling relationships predict that the behavior of the models should be similar if the flow rates are within a ratio of 2.5 to 1. Thus the 3.0-gpm test of Model I should, under a scaled heat load, be the same as the 7.5-gpm Model II test. However, the test results do not indicate this; instead they indicate that a non-linear relationship may exist between the two models.

If we assume that a flow rate range of 3.0 to 4.0 gpm in Model I actually corresponds to the 4.75- to 7.5-gpm zone of Model II (rather than the predicted zone of 7.5 to 10.0 gpm) a similarity in results emerges. Under such a relationship both models would then exhibit an average outlet water temperature which increases to a relative maximum at low flow rates, decreases to a relative minimum at intermediate rates and again increases prior to leveling-off at even higher flow rates thereafter. With outlet water temperatures dependent upon both flow rate and density influences, a linear scaling relationship is not very probable and as such can only be used as a guideline. A method of predicting possible nonlinearities in the flow rate scaling is discussed in the section which presents the approximation of the heat transfer coefficient. It should be emphasized that the curves in Figure 11 are not to be construed as exact but only as indicative of general variations in temperature between different flow rates.

Although little information is available concerning the heat and mass transfer at an ice/water interface under conditions exactly comparable to those of the

heat sink, the work of Vanier<sup>18</sup> concerning natural convective melting along a vertical ice sheet does provide some insight as to why a minimum temperature might occur within this range of flow rates. Vanier noted that the net direction of water movement was upward for certain ranges of bulk water temperature, a direct result of the density inversion of water. In addition he observed the existence of zones where the net motion was downward, as well as zones of dual flow in which water flowed in both directions. The range of these dual zones tends to be rather narrow, as is illustrated in Figure 12 which is reproduced from his paper.

In the ice-water heat sink the gross flow direction is always downward; that is, heated water is added at the top and the same quantity is removed from the bottom. As discussed previously, at extremely low flow rates the water appears to move downward in a horizontal layer, and at the highest flow rates it moves as conventional flow through an annular space. These observations indicate that a transition occurs as the flow rate increases. The density influences which produced stratification at low flow rates could, at some intermediate rate, provide sufficient resistance to the annular flow process to generate an unstable condition where the motion of water alternately traveled upward and downward, dependent upon fluctuations in the bulk water temperature. Such a phenomenon would result in fluctuation in the outlet water temperature similar to that observed in test 4, namely an increase in temperature up to the

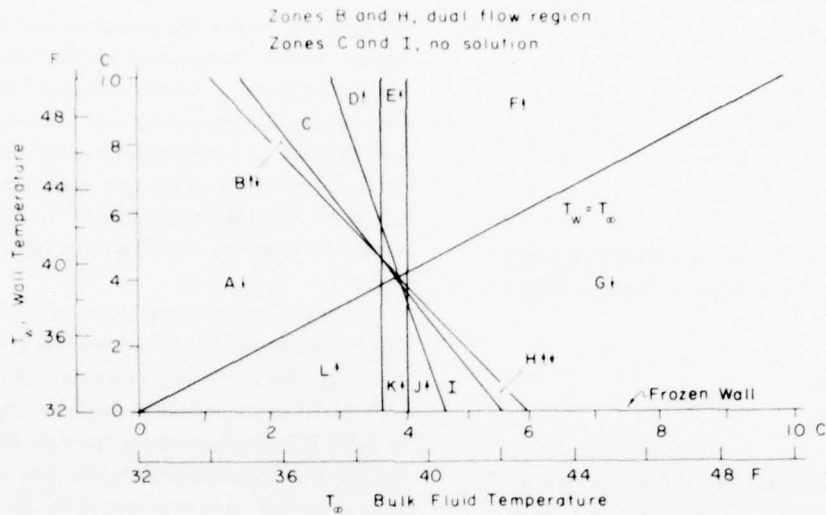


Figure 12. Flow zones (after Vanier<sup>18</sup>).

maximum density, followed by a sudden decrease in temperature as the flow reversed.

Since

### Approximation of the rate of melting

The observed change in water level with time during each experiment can easily be converted to a gross rate of melting. Since the total mass of the system  $M_s$  remains constant, then

$$M_{\nu} = M_i + M_{\infty}$$

where  $M_i$  is the mass of ice in sink (lbm), and  $M_w$  is the mass of water in sink (lbm). Thus

$$\frac{dM_s}{dt} = 0 = \frac{dM_i}{dt} + \frac{dM_w}{dt}$$

OR

$$\frac{dM_w}{dt} = - \frac{dM_i}{dt} .$$

Similarly, if the ice remains submerged, then the total volume  $V$  is given by

$$V_1 = V_1 + V_2$$

where  $V_i$  is the ice volume ( $\text{ft}^3$ ) and  $V_w$  is the water volume ( $\text{ft}^3$ ). Thus

$$\frac{dV_t}{dt} = \frac{dV_i}{dt} + \frac{dV_w}{dt} \quad .$$

where  $\rho_i$  is the density of ice and

$$M_{\text{av}} = \rho_{\text{av}} V_{\text{av}}$$

where  $\rho_w$  is the density of water, then for constant densities

$$\frac{dV_i}{dt} = \frac{1}{c_i} \frac{dM_i}{dt}$$

and

$$\frac{dV_w}{dt} = \frac{1}{c} \frac{dM_w}{dt}.$$

Upon substitution, this yields

$$\frac{dV_t}{dt} = \frac{1}{\rho_i} \frac{dM_i}{dt} + \frac{1}{\rho_w} \frac{dM_w}{dt}.$$

Using the above relationship between the rates of change in ice and water, we have

$$\frac{dV_t}{dt} = \left( \frac{1}{a} - \frac{1}{a_i} \right) \frac{dM_i}{dt}$$

83

$$\frac{dM_i}{dt} = \left( \frac{\rho_w \rho_i}{\rho_w - \rho_i} \right) \frac{dV_t}{dt}$$

Since

$$V_t = \pi R^2 H$$

where  $R$  is the radius of the heat sink tank (constant) (ft) and  $H$  is the depth of water in the tank (variable) (ft).

$$\frac{dV_t}{dt} \approx \pi R^2 \frac{\Delta H}{\Delta t}$$

where  $\Delta H$  is change in water level during the time increment  $\Delta t$ . Therefore, the rate of melting can be approximated by

$$\frac{dM_i}{dt} \approx \pi R^2 \left( \frac{\rho_w \rho_i}{\rho_w - \rho_i} \right) \frac{\Delta H}{\Delta t} \quad (6)$$

The changes in water level for each test are shown in Appendix A, Figures A1-A5. It should be noted that the water level decreases during melting since ice has a lower density than water. Once the ice has completely melted, the water level increases as a result of the decrease in water density with increasing temperature.

In the above derivation it is assumed that the density of the water remains constant; this is not precisely true because, as melting proceeds, there is an increase in the bulk water temperature. However, this temperature increase is small and the assumption introduces only a small error. The bulk water temperature  $T_b$  is approximated as the numerical average of the inlet and outlet water temperatures; that is

$$T_b = \frac{1}{2n} \sum_1^n (T_{in} + T_{out}) \quad (\text{°F}) \quad (7)$$

where  $n$  is the total number of temperature readings taken from the start of the test until completion of melting.

Although eq 7 represents a rather crude approximation of the bulk water temperature, large changes in the bulk water temperature result in only small errors in the rate of ice melting. For example, if the bulk water temperature were calculated to be 40°F but was actually 50°F, the density factor would change by a mere 0.6%. In this example the ice density was taken as 56.7 lbm/ft<sup>3</sup>, rather than the standard 57.2 lbm/ft<sup>3</sup>.

for clear ice, because the air bubbling system caused entrainment of a large number of air bubbles in the ice and thus reduced its density. (Figure 9 shows air bubbles released during melting.) By comparing the initial ice volume prior to any melting to the total change in volume for the sink, it was determined that the density of the ice varied from 56.6 lbm/ft<sup>3</sup> to 56.9 lbm/ft<sup>3</sup> for the six tests, the overall average value being 56.7 lbm/ft<sup>3</sup>.

Using a 10-hour interval in the preceding approximation equation, the rate of melting was determined for each test. These results are plotted in Appendix Figures A1-A5 and tabulated in Table IV. Also included in Table IV is a gross melting rate determined by dividing the total initial ice mass by the time required to melt all the ice. A comparison of the gross melting rate to the average value of the approximated melting rate shows a high degree of correlation.

A comparison of the melting rates for the different tests, as in Figure 13, is complicated by the fact that the applied heat rejection rate varied for each test (see Table II). For example, in converting the rate of melting into a rate of heat exchange (i.e. each pound melted required 144 Btu), the heat rejection rates for the first 10-hour intervals ranged from 31,536 Btu/hr to 41,184 Btu/hr. These values represent only the latent heat portion of the total heat added to the sink; some heat is stored by sensible heating of the water initially in the annulus and the melted water generated during the interval. The percentage of stored sensible heat varies with time from only about 2% during the early stages of heat rejection up to about 50% during the later stages of melting. It should also be noted that the water table elevations in the tank were measured within  $1/16$  in. of the true value, so that a maximum error of  $1/8$  in. or approximately 7% was possible.

In reviewing the data presented in Table IV (except for the results of test 4) all melting rates lie within a tolerance band of approximately 10% of the average rates. After 30 hours of operation there is an even smaller variation in melt rate among the various tests, indicating that flow rate effects are not significant in the final hours of the melting process. It is during this period that the remaining ice exists in a small mass at the tank centerline, producing a large annular passage for water flow and thus a substantial reduction in the water velocity. The flow rate influence, manifested by the ice profiles (Fig. 8), exerts a decreasing influence as more ice is melted, until a point is reached when all sinks begin to exhibit the same basic melting rate.

Table IV. Melting rates - Model II.

Test no.	Flow rate (gpm)	Melting time (hr)	Melting rate during time interval of approximation						Avg of approx. rate (lbm/hr)	Gross melting rate* (lbm/hr)
			0-10	10-20	20-30	30-40	40-50	50-60		
1A	4.73	63	249	242	235	220	198	176	220	210
1B	4.73	65	286	264	227	205	191	161	222	204
2	2.50	56	236	228	228	206	184	**	216	219
3	10.00	58	286	271	242	213	176	**	238	220
4	7.50	67	219	205	183	176	169	197	192	193
5	13.50	60-63 <sup>†</sup>	249	227	227	213	191	147	209	218
Average values <sup>††</sup>			261	246	232	211	188	161	216	211

\* Gross melting rate =  $\frac{\text{Initial ice mass}}{\text{Total melting time}}$

<sup>†</sup> Precise value unknown due to equipment failure, mean value of 61.5 hours used to calculate gross melting rate.

<sup>\*\*</sup> Melting completed during interval.

<sup>††</sup> Average excluding test 4.

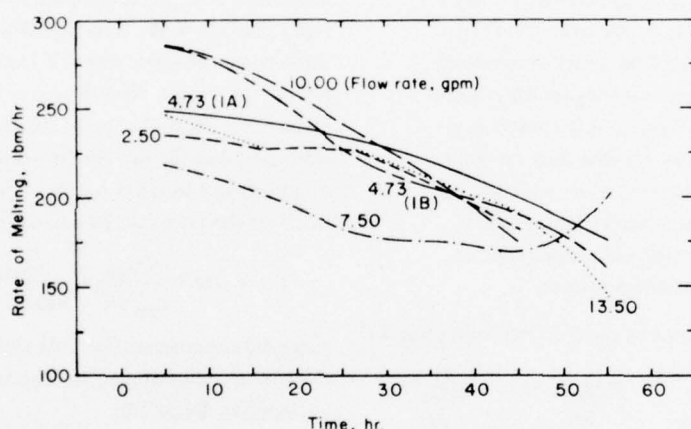


Figure 13. Melting rates for Model II.

The variations in melting rate during the initial hours probably result primarily from different rates of heat rejection and different initial ice temperatures, rather than from differences in flow rates. During this period less than 5% of the rejected heat is stored as sensible heat; thus the rate of melting is almost identical to the rate of heat rejection. For example, the differences in melting rate for the two 4.73-gpm tests result from different initial ice temperatures. In test 1A the initial average bulk ice temperature was 17.6°F, while in test 1B it was 31.4°F. As indicated by Figure 13 and Table IV, the test with the lower ice temperature stored a greater amount of its rejected heat in the sensible heating of the ice. Yet both tests show a parallel relationship during the later hours of

operation, indicating that the melting rate eventually becomes independent of the initial conditions. In a similar manner the variations depicted in the other tests during the initial hours most likely result from different heat loads.

The results of the 7.50-gpm test tend to illustrate a possible reduced heat rejection rate. Although, for this test, the average heat rejection rates shown in Table II do not indicate a low heat rejection rate, the very low rate of ice melting does imply this to be the case.

Using the average melting rate data from Table IV, it is possible to show the partitioning between the amount of heat rejected to the ice and to the water for each 10-hr interval. Because of its much lower

melt rates, test 4 (Model II-7.50 gpm) will be excluded from the average. During the first 10 hours the average gross rate of melting is 261 lbm/hr. With the rate of melting known, the rate of heat storage associated with melting can be determined, since 144 Btu is required to melt each pound of ice. Using both the nominal applied heat load of 42,013 Btu/hr and the average rate of 37,760 Btu/hr shown in Table II, the percentage of total heat involved in ice melting can be derived. Table V lists results of this calculation.

These results indicate that, on the average during the initial 10-hr period (representing about 16% of the total melting time), between 90% and 99% of the rejected heat is involved in melting ice. During the last 10-hr period, an average of between 55% and 60% of the rejected heat is involved with ice melting.

If flow rate effects exist, they apparently do not have any significant influence on the overall rate of melting. Rather, the effect of flow rate is manifested by the outlet water temperature during melting, a result of the degree of overall mixing of the water as it passes through the sink. Thus, for low flow rates the slight degree of mixing of the inlet water with the melt water results in low outlet water temperatures. As flow rate is increased, mixing effects increase, resulting in higher outlet water temperatures.

Table V. Rates of heat rejected to the ice (excluding test 4).

Time period (hr)	Rate of melting* (lbm/hr)	$Q_i t$ (Btu/hr)	$\dot{Q}_i / \dot{Q}_{nom}^{**}$ (%)	$\dot{Q}_i / \dot{Q}_a^{††}$ (%)
0-10	261	37,613	89.5	99.5
10-20	246	35,482	84.5	94.0
20-30	232	33,379	79.4	88.3
30-40	211	30,442	72.5	80.6
40-50	188	27,072	64.4	71.6
50-60	161	23,232	55.3	61.5

\* Data from Table IV. \*\*  $\dot{Q}_{nom} = 42,013$  Btu/hr (nominal value).  
 †  $\dot{Q}_i = 144 dM_i$ . ††  $\dot{Q}_a = 37,760$  Btu/hr (Table II).

#### COMPARISON OF EXPERIMENTAL AND COMPUTED RESULTS

As important as the determination of the operating characteristics of the heat sink may be, it is of equal importance to determine how accurately these characteristics can be predicted. A computer program developed during the Model I study<sup>3</sup> was used to make these predictions. In this report the following factors are used as a basis for comparison: mean outlet water temperature during the melting period, overall time required to complete melting, and behavior of the

outlet water temperature after all the ice is melted. Due to the possible variations in heat rejection rate for the different tests, two computer solutions were developed for each test. One used a heat rejection rate equal to the value determined by the previously mentioned Procedure 1 — involving the measurement of the coolant water flow rate and the temperature difference maintained between the inlet and the outlet. The other solution used the heat rejection rate for the lower of the values determined either by Procedure 2 (the heat balance technique) or Procedure 3 (the slope of the outlet temperature-time curve). This established the most probable band of heat rejection rates for the actual test.

When the computer solution is calculated using the minimum heat rejection rate as determined by Procedure 2 or 3, it is necessary to adjust either the input coolant water flow rate  $W$  or the temperature difference across the sink  $\Delta T$  from the nominal experimental values. The flow rate was selected for adjustment because the larger number of temperature readings taken during the tests led to a higher degree of confidence in these results. The adjustment was made to the flow rate by use of the equation:

$$\text{Flow rate} = \frac{\dot{Q}_{min}}{c_{pw} \Delta T} = \frac{\dot{Q}_{min}}{500.15 \Delta T} \quad (\text{gpm}). \quad (8)$$

Table VI summarizes the heat rejection rates used for the various computer runs. The adjusted flow rates are listed in Table VIb.

Table VI. Summary of computer predictions.

Test no.	Heat rejection rate (Btu/hr)	Flow rate (gpm)	Mean temp		Melting time (hr)
			inlet (°F)	outlet (°F)	
<b>a. Maximum heat rejection rate (<math>\dot{Q}_{max}</math>)</b>					
1A	41,305	4.73	43.6	60.8	61.5
1B	40,150	4.73	43.3	60.0	62.5
2	41,140	2.50	40.2	72.7	58.5
3	41,410	10.00	45.8	53.9	57.5
4	42,090	7.50	44.9	55.2	56.5
5	40,260	13.50	46.1	52.0	61.5
<b>b. Minimum heat rejection rate (<math>\dot{Q}_{min}</math>)</b>					
1A	38,600	4.41*	42.3	59.6	64.5
1B	35,050	4.12*	41.8	58.6	70.5
2	40,720	2.43*	39.8	72.3	60.5
3	38,530	9.30*	45.0	53.1	61.5
4	35,920	6.40*	43.3	54.4	67.5
5	34,790	12.66*	45.3	51.2	64.5

\* Flow rate adjusted using eq 8.

In Appendix Figures A1-A5 the computer-predicted outlet water temperatures have been plotted

with the comparable experimental test. Inlet temperature curves for the computer solutions have been eliminated in these figures since they differ from the outlet by a constant, the  $\Delta T$  shown in Table III.

Table VII and Figure 11a illustrate the variation between the computer predictions and the experimental observations. Generally, the computer version predicts a higher mean outlet water temperature during the melting process for both heat rejection rates. It had been expected that the use of the two heat rejection rates might result in the predicted temperatures bracketing the observed values. Although the computer program did not predict the inflection in outlet water temperatures which occurred in the neighborhood of 7.5 gpm, it otherwise reasonably replicated the overall increasing trend in outlet water temperature with increasing coolant water flow rate. This indicates that the computer model simulates the gross process well but predicts a slightly greater amount of mixing of the inlet water and the water within the sink.

**Table VII. Average outlet water temperature during melting: experimental results and computer predictions.**

Test no.	Measured ( $^{\circ}$ F)	Predicted from $Q_{max}^*$ ( $^{\circ}$ F)	Predicted from $Q_{min}^*$ ( $^{\circ}$ F)
1A	40.8	43.6	+6.7
1B	41.2	43.3	+4.9
2	38.5	40.2	+4.5
3	43.4	45.8	+5.4
4	40.3	44.9	+11.3
5	43.6	46.1	+5.8
Average error		+6.4%	+3.9%

This tendency to predict a higher degree of mixing is well-illustrated in the low flow rate tests after all ice has been melted. During the experimental tests it was observed that the predominant feature of the post-melting period was the density controlled flow of water through the sink. This was manifested by the motion of convective water cells in the heat sink tank. As the test flow rates were increased it was noted that the density influences had a decreasing influence on the post-melting period until at 7.50 gpm the effects were completely absent.

However, for the lowest flow rate the computer prediction of the outlet water temperature-time history shows only slight fluctuations of the type associated with density influences. These predicted fluctuations

are more representative of the type found at the next higher flow rate (4.73-gpm) experimental test. This leads to the conclusion that the flow process used in the computer program errs slightly in predicting the density-related flow effects and tends to predict a greater amount of mixing of the water within the sink than actually occurs. This limitation in the accuracy of the prediction does not present a serious drawback, since during this period it is rather easy to predict the behavior of the outlet water by using the simple relationships developed in the previous section.

Except for the deviation cited above, the computer program does simulate the behavior of the sink with a high degree of accuracy. The errors which do occur tend to be conservative, as they predict higher than actual outlet water temperatures. When the prediction is coupled with the operation of a simulated condenser module, a somewhat lower system capacity will be predicted than is actually available. Assuming no other scaling effects are encountered with much larger heat sinks, it appears that the computer program could be used to predict the outlet temperature-time curve for a prototype sink. The actual outlet water temperature would be slightly lower than predicted, resulting in a higher overall system efficiency and subsequently a slightly increased overall capacity. The magnitude of this modest increase in capacity would actually depend upon the sensitivity of the plant's efficiency to the coolant water temperature. Thus the error in the prediction of outlet water temperature can be considered to be a small inherent safety factor in the selection and sizing of a prototype system.

A comparison was also made between the predicted time required to melt all the ice by using both the high and low heat rejection rates discussed earlier and the time measured in the test model. These results are presented in Table VIII. The high heat rejection rate results in a predicted melting time which is 2.2% less than that observed, while the lower rate predicts a melt time which is 5.1% greater than that observed. Since the use of these limiting values of heat rejection rate tends to bracket the experimental results, it is reasonable to conclude that the program is predicting the ice melting times rather accurately. The prediction of a higher outlet temperature than observed can be attributed to inability of the computer program to provide for the effect of water density inversion on the flow process. It can be concluded that the

**Table VIII. Comparison of melting times of experimental and computer models.**

Test no.	Measured* (hr)	Predicted from $Q_{max}$ (hr)	Predicted from $Q_{min}$ (hr)
1A	63	61.5	-2.4
1B	65	62.5	-3.9
2	56	58.5	+4.5
3	58	57.5	-0.9
4	67	56.5	-10.5
5	60-63†	61.5	0.0
		Average error	-2.2%
			+5.1%

\* Corrected to account for initial ice temperatures below 32°F.

† Precise value not known due to equipment failure; mean value of 61.5 hr used to calculate percentage error.

computer program tends to predict a greater amount of mixing of inlet with outlet water than will actually occur, the differences most likely resulting from the density inversion of water.

#### COMPARATIVE ANALYSIS OF THE MODEL SINKS

The first experimental investigations of the ice-water heat sink concept employed a test apparatus 4 ft in diameter by 6 ft high (Model I). These initial studies indicated that the ice-water heat sink concept was both feasible and practical and merited further investigation. The results of these prior studies are presented in references 3 and 14. The scaling relationships developed by Brown and Quinn<sup>3</sup> were used to establish the experimental heat rejection and coolant flow rates. Since the comparison of the model sinks is based upon these scaling relationships, some discussion of their inherent limitations is in order.

Based mainly on geometric considerations, the scaling relationships were developed to ensure similarity in the operational characteristics of different size sinks. This would include parameters such as the rate at which heat could be rejected to the sink, the relationship between the heat rejection rate, coolant water flow rate and outlet water temperature, and useful life of the sink. Mathematical difficulties involved in modeling dynamic effects, such as the density inversion of water and boundary layer flow, precluded their inclusion in the relationships. It was felt that these influences would be of secondary importance compared to the

general heat transfer process and that simplified scaling relationships could be employed to relate the models with a reasonable degree of confidence.

In comparing the two models the expectation was not to find a perfect correspondence in test results but rather similarities in behavior, such as the melting pattern, general temperature-time history of the outlet water, and predictability by use of the computer program. Minor differences in the performance of comparable tests in the two model studies would not be considered a serious limitation, as variations in the initial test conditions were sufficiently large to prevent exact correlations.

In the following discussions the "Model I tests" refer solely to the 16,805-Btu/hr tests conducted using the 4-ft-diam model, and the "Model II tests" refer to the 42,013-Btu/hr tests conducted using the 6-ft-diam apparatus. Although many of the results developed during the earlier Model I studies are presented in this report, the reader should consult references 3 and 14 if additional information is needed.

The technique for measuring melting times differed in the two test series. In the Model I study, the melting time was determined by monitoring thermocouples and by direct observation. This technique does not give the exact time at which melting was completed but rather it shows the earliest time at which ice was no longer visually observed in the tank. With an interval of about 4 hr between observations, it is possible that melting may have been completed 2 to 3 hours prior to the observed "melting time." In the Model II studies melting was monitored by measuring changes in the water level and by temperature measurements. Interpolation between points on the water table graph (Fig. A1-A5) results in a finer measurement of the exact melting time. In addition the temperature measurements show a high degree of correlation with this method. During the final hour of melting a small zone of low temperature water exists in the vicinity of the remaining ice; this zone is located along the vertical centerline of the tank at approximately  $1/3$  of its height. Once the ice is completely melted, the temperature of this zone rapidly increases to the mean temperature of the water surrounding the zone. For the higher flow rate tests the occurrence of this sudden temperature change coincides with the abrupt change in the behavior of the water level graphs. In the lower flow rate tests, where

density stratification effects are present, the rise in temperature of this zone occurs slightly after the inflection in the graph of the water level, the difference normally being 1 to 2 hours. It is felt that the Model II melting times are known to within an hour of the actual, representing a relative error of one hour in sixty. In the Model I studies melting times could vary by two to three hours, for a relative error of two hours in forty (with the observed melt time always longer than the actual).

Such variations in procedure result in differences not only in the melting time parameter but also in other parameters used to compare the models. For example, in calculating the average outlet water temperature during melting, it is averaged up to and including the temperature at which melting is completed. Since in the final hours the outlet water temperature shows a continuously increasing trend, the use of a melting time later than the actual will increase the average value; this amounts to about 4 to 5% for each two hours added. Similarly any parameter dependent upon the melting time would be affected by this difference in procedure.

To show the relationships between the tests and in the two model sinks, Table IX illustrates the flow rate scaling which is based on the work originally reported in reference 3 and repeated in Appendix B of this report.

**Table IX. Flow rate scaling for Models I and II.**  
(Scaling after ref. 3.)

Model I		Model II	
Test no.	Flow rate (gpm)	Test no.	Flow rate (gpm)
1S <sub>1</sub> , 1S <sub>2</sub>	1.89	1A, 1B	4.73
2S	1.00	2	2.50
3S	4.00	3	10.00
4S <sub>1</sub> , 4S <sub>2</sub>	3.00	4	7.50
5S	0.62	*	1.55*
*	5.40*	5	13.50

\* No tests conducted at these values.

The predominant feature of the low flow rate tests was the development of a stratified flow process involving the convective motion of water cells through the sink. Evident in both models this indicates a direct similarity in the flow pattern between the 1.00-gpm Model I test and the 2.50-gpm Model II test. The inlet and outlet water temperature-time histories for both

tests are shown in Figure 14. A time scaling factor of 1.5 is used to provide a comparable time basis; in other words the actual times for the Model I test are multiplied by 1.5 (see App. B for derivation of the scaling factor) to convert them to Model II times. Both tests have a relatively constant temperature period which ends soon after melting is completed. At this point there is a sudden increase in outlet water temperature to the temperature of the inlet water a few hours earlier; this is felt to be due to the arrival of the water cell at the outlet. Although the tests were ended soon after melting was completed, it is believed that with a constant  $\Delta T$  maintained between inlet and outlet, the inlet water begins to form another convective water cell at the top of the sink which travels downward in a similar manner to produce a second constant temperature period, followed by another sharp rise in outlet water temperature. If this were not true, i.e. if the water began to store the rejected heat by mixing, the outlet water temperature curve would have approached a constant slope line similar to the higher flow rate tests.

Overall, the outlet water temperatures for the Model I and II low flow rate tests show a high degree of correlation, the average values for the melting periods differing by less than 1.5°F. If a scaling factor of 1.5 is used for the time axis, both sinks reach the same temperature-time coordinate at approximately the same relative percentage of their operating time. This tends to confirm the general applicability of the scaling factors for low flow rates for the two sinks studied.

The next higher flow rate tests, those of 1.89 gpm in Model I and 4.73 gpm in Model II, show an almost exact correlation between the two models (Fig. 15). The outlet water temperature during the melting period is identical for the two models; once melting has been completed, both tests experience the slight fluctuations in the slope of the outlet curve associated with the transition from a density-influenced flow to a mixed flow.

Thus, in the lower flow rate range, the scaling relationships appear to provide an accurate method for relating different size sinks; however, results from the intermediate flow rate tests indicate that these relationships may not be used for all flow rate conditions. The results of the intermediate flow rate tests for 3.00 gpm in Model I and 7.50 gpm in Model II are shown in Figure 16. Except for the initial hours of operation, distinct differences in sink behavior occur.

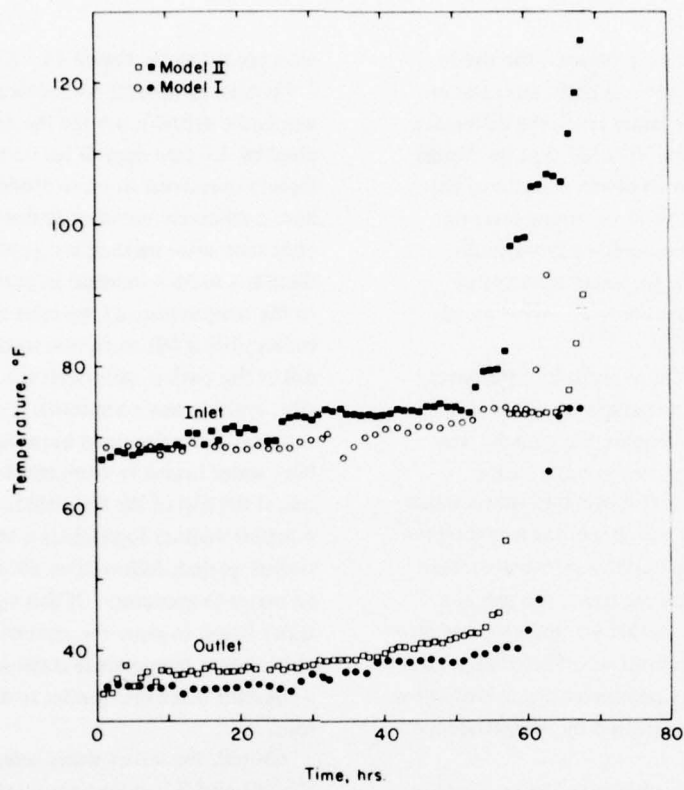


Figure 14. Comparison of 2.50-gpm Model II test to 1.00-gpm Model I test.

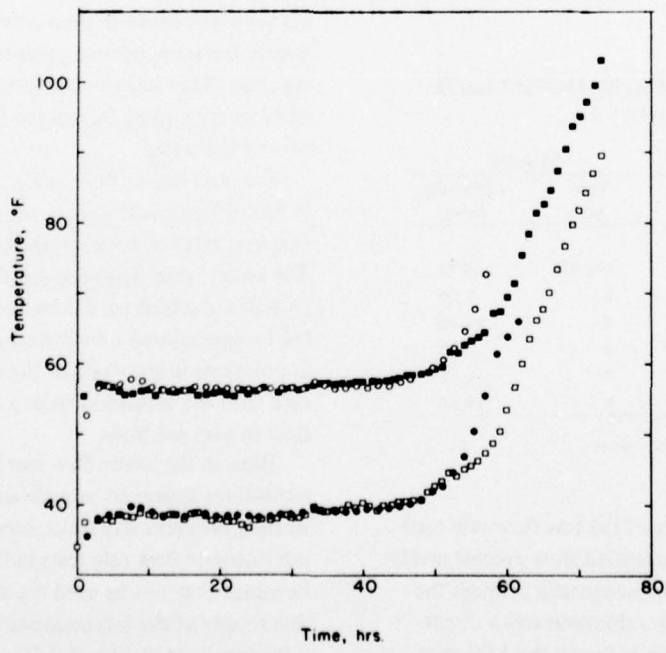


Figure 15. Comparison of 4.73-gpm Model II test to 1.89-gpm Model I test.

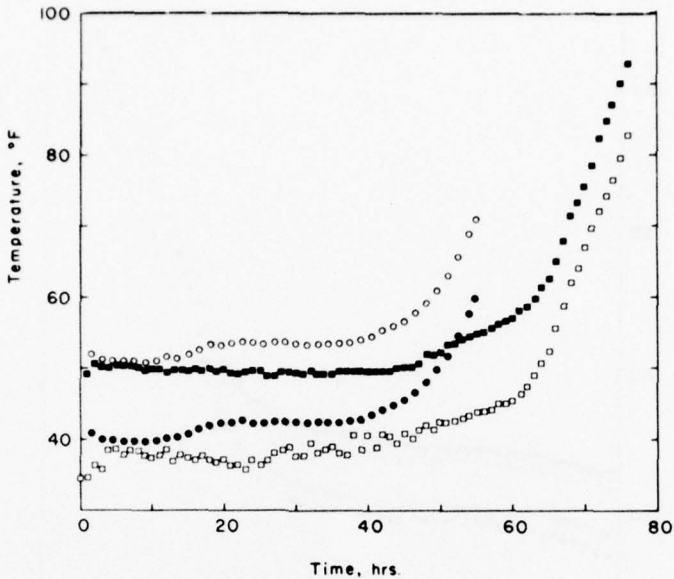


Figure 16. Comparison of 7.50-gpm Model II test to 3.00-gpm Model I test.

With two tests conducted at the 3.00-gpm rate during the Model I study, the rather sudden rise in outlet water temperature at the 15th hour (Model II time) during the melting period was substantiated. As noted earlier, the possible low heat load during the melting period in Model II could have caused the low outlet water temperature observed.

A comparison between the highest flow rate tests, 4.0 gpm in Model I and 10.0 gpm in Model II, is illustrated in Figure 17. An almost constant difference in outlet water temperature exists between these two tests. This difference, on the order of one to two degrees, indicates that the same general behavior is occurring in each, but that a slight difference exists either in the partitioning of the rejected heat between the ice and water or in the overall amount of inlet water mixing with the water in the sink. This is also illustrated in Figure 11 which compares the average outlet water temperatures during melting. In the Model I tests there is a decrease in average outlet water temperatures between 3.0 gpm and 4.0 gpm, while for the Model II tests the comparable flow interval from 7.5 gpm to 10.0 gpm exhibits an increase. In turn this indicates that the scaling relationship between the models for this flow rate interval is not correct but requires additional factors. The data for the two models would exhibit a higher degree of correlation if the flow rate interval of 3.0 to 4.0 gpm in Model I were scaled to correspond to an interval of 5.5 gpm to 8.0 gpm in Model II, rather than the interval of 7.5

gpm to 10.0 gpm determined from the scaling relationships in Appendix B. A more detailed discussion of possible nonlinearities in the scaling will be given in the section concerning the approximation of the heat transfer coefficient.

Although a comparable high flow rate test was not conducted during the Model I study, the 13.50-gpm test of Model II indicates an interesting trend in average outlet water temperature during the melting period. Between the interval of 10.0 gpm and 13.50 gpm the average outlet water temperature becomes essentially constant at a value of  $43.5^{\circ}$  (Fig. 11a). This does not mean that during the melting period the outlet water temperature is constant (Fig. 17), but that the average value over the entire melting interval approaches a constant. Should this trend continue for even higher flows, then modeling of the prototype sink and condenser unit is simplified.\*

\* The similarity between the outlet temperature-time curves for the 10.00- and 13.50-gpm tests is depicted on Figure 10. The somewhat greater ice mass in the 13.50-gpm (Table I) is responsible for the difference in melting times. Should this relation hold for even higher flow rates the effect of flow rate on the relationship between outlet temperature and time could be ignored and a "standard" outlet water temperature-time curve could be prepared independent of flow rates above the 10.00-gpm level, or the appropriately scaled value for another size heat sink.

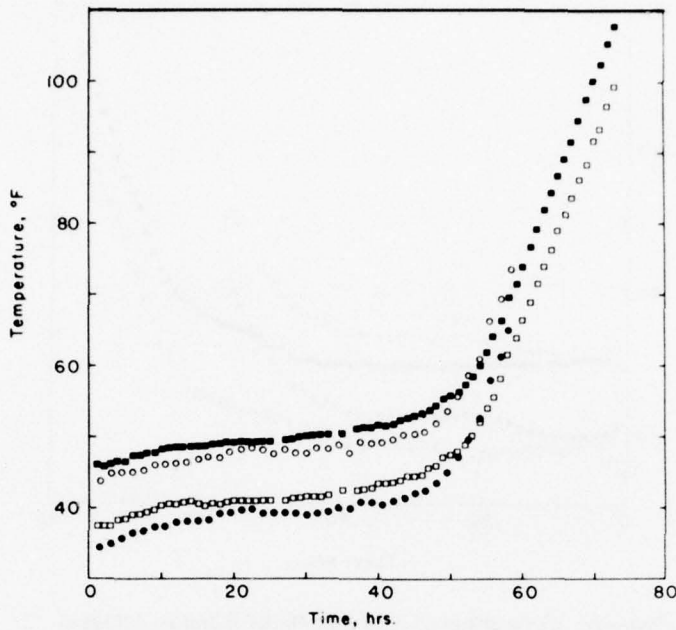


Figure 17. Comparison of 10.00-gpm Model II test to 4.00-gpm Model I test.

Comparison of the Model I experimental results to those predicted by the computer program is discussed in reference 14. In general the same type of variations observed between the Model II experimental and computer results also occurred in the Model I study (see Fig. 11b). The computer program tends to predict outlet water temperatures slightly higher than those observed and thus represents a conservative prediction for both Model I and Model II operating characteristics.

#### APPROXIMATION OF THE HEAT TRANSFER COEFFICIENT

From the first conceptual studies of the ice-water heat sink through the most recent experimental test programs, it has been recognized that information relating the heat transfer coefficient to the water temperature and flow conditions of an annular flow sink would be necessary to accurately predict the behavior of a prototype installation. With little information available concerning the heat and mass transfer at an ice/water interface under conditions similar to those in the heat sink, a series of progressively more rigorous methods have been made to approximate the heat transfer coefficient by using the experimental data.

The first method, reported in reference 14, used a very simplified geometric analysis of the melting process by assuming that the ice cylinder melted uniformly along the entire vertical surface with a constant rate of change in radius. To permit a comparison of the results of the previously utilized approximation with the refined method developed in this report, a brief discussion of the earlier techniques is presented. A rather simple relationship was developed to estimate the heat transfer coefficient by using test data from the Model I tests. In functional form the relationship developed (see App. C for derivation) was

$$h = \frac{\rho_i L}{\Delta T_m} \frac{\Delta R}{\Delta t_m} \quad (9)$$

where  $h$  = average heat transfer coefficient (Btu/hr ft<sup>2</sup> °F)

$\Delta R$  = total change in radius of the ice cylinder (ft)

$\Delta t_m$  = melting time (hr)

$\Delta T_m$  = mean temperature difference between the ice and the water (°F)

$L$  = latent heat of ice (144 Btu/lbm).

It must be emphasized that, in this approximation, the rate of change in radius was assumed to be constant and equal to the total change in radius (from the initial value of 2 ft to zero) divided by the time required to melt all the ice.

When this equation was employed in reference 14 to calculate the heat transfer coefficients, the melting time used in the relationship was not the observed, but rather an effective, melting time. It was reasoned that sensible heating of the water, rather than ice melting, was the predominant mode of heat storage during the final hours of melting when the outlet water temperature began to increase rapidly. Thus it was assumed that ice melting had essentially terminated at the time that the outlet began to increase in temperature and not necessarily when ice was no longer present in the heat sink. For the low coolant water flow rate tests the effective melting time agreed well with the observed melting time, but in the higher flow rate tests the effective melting time was three to five hours less than the observed values.

The measurement of melting rates for the Model II tests casts serious reservations on the use of this effective melting time. Unlike the assumed behavior, the actual melting rates indicated that significant amounts of ice are still being melted even during the final hours of melting (see Table II). These results indicated that sensible heating does not become the predominant mode of heat transfer until essentially all the ice is melted, even though the outlet water temperature has begun to increase before that time. While this might seem to be a contradiction (i.e. if the water temperature is increasing, sensible heating must occur), it must be emphasized that the behavior of the outlet water is not synonymous with the behavior of the bulk of the water in the test tank. Specifically, sensible heating is manifested by an increase in the bulk water temperature, and changes in the bulk water temperature are not necessarily reflected by changes in the outlet water temperature. This behavior is most evident in the lowest flow rate tests where the outlet water temperature remains constant although heat is rejected to the sink.

The effect of this change in melting time of the heat transfer coefficients for the Model I tests is illustrated in Figure 18. Unlike the earlier results which indicate that as the flow rate increases the heat transfer coefficient increases, the revised values indicate

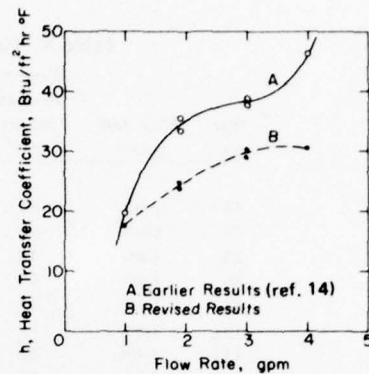


Figure 18. Heat transfer coefficients for Model I, 16,805 Btu/hr tests.

that the overall heat transfer coefficient tends to approach a constant value.

The revised heat transfer coefficients have also been tabulated in Table X for all Model I tests. These values should be used instead of the values presented in reference 14. Also reported in reference 14 was a compilation of Nusselt numbers for the melting process vs the test flow rate. As for the heat transfer coefficient these values represented overall average values for the entire melting process. In calculating the Nusselt number the characteristic dimension selected was the diameter; in the calculations of reference 14 the numerical value assigned to the diameter was the initial value of 4 ft. As will be shown later in this section other selections for the characteristic dimension can be made which result in a better correlation of the data.

Due to the complex melting and flow processes in the heat sink, certain limitations or restrictions are inherent in any set of assumptions employed to determine heat transfer coefficients. In this first approximation technique the major limitation or discrepancy occurs as a result of the assumption that the rate of change in radius remains constant as the ice cylinder melts. To illustrate the influence of this assumption on the melting process, it is fairly simple to develop an expression relating the change in radius to time. In this example, nominal values from the Model II tests will be used, since the rates of melting for these tests were measured and can be compared.

Table X. Heat transfer coefficients for Model I.

Test no.	Flow rate (gpm)	Time to melt all the ice (hr)	Bulk water temp (°F)	Mean temp diff between ice and water (°F)	Heat rejection rate (Btu/hr)	Heat transfer coefficient (Btu/ft <sup>2</sup> hr °F)
5S	0.62	36	69.5	37.5	20,032	12.00
7S	0.66	56	54.9	22.9	11,272	12.71
2S	1.00	43	53.7	21.7	15,200	17.48
6S	1.89	78	45.0	13.0	8,425	16.13
8S	1.89	35	53.4	21.4	29,520	21.79
1S <sub>1</sub>	1.89	41	48.0	16.0	16,720	24.83
1S <sub>2</sub>	1.89	40	49.0	17.0	18,320	23.93
4S <sub>1</sub>	3.00	33	48.6	16.6	16,848	30.18
4S <sub>2</sub>	3.00	36	47.9	15.9	16,776	28.97
3S	4.00	40	45.4	13.4	16,350	30.47

If it is assumed that the change in the radius of the ice cylinder is uniform over the length and occurs at a constant rate, then

$$\frac{dR}{dt} = \text{constant} = C_1.$$

The functional relationship between the radius and time in operation can be found from direct integration. Thus

$$R(t) = C_1 t + C_2.$$

With the boundary conditions that at time zero  $R(t)$  is equal to the initial value  $R_0$ , and at the melting time  $t_m$ ,  $R(t)$  is zero, the constants  $C_1$  and  $C_2$  can be evaluated. This results in a solution of the form

$$R(t) = R_0 \left( 1 - \frac{t}{t_m} \right). \quad (10)$$

Since it is also assumed in the approximation that melting occurs only radially along the cylindrical surface and not in the vertical direction, the volume of ice melted at any time  $t$  can be found from

$$V_m(t) = \pi H_0 [R_0^2 - R(t)^2] \quad (\text{ft}^3) \quad (11)$$

where  $H_0$  is the initial height of the ice cylinder (ft).

For the Model II tests the average values of the constants appearing in eq 10 and 11 are

$$R_0 = 3.0 \text{ ft}$$

$$H_0 = 8.6 \text{ ft}$$

$$t_m = 61.76 \text{ hr (Table IV).}$$

Thus

$$R(t) = 3.0(1 - 0.016t) \quad (10a)$$

and

$$V_m(t) = 243 - 27[R(t)]^2. \quad (11a)$$

Therefore, after the first 10 hr of an average Model II test the radius would be approximated as

$$R(10) = 2.51 \text{ ft}$$

and the volume melted would be

$$V_m(10) = 27.0[(9) - (2.51)^2]$$

$$V_m(10) = 72.9 \text{ ft}^3.$$

To estimate the rate of melting the rate of change of volume can be approximated by

$$\frac{dV_m}{dt} = \frac{V_m}{\Delta t} = \frac{72.9 \text{ ft}^3}{10 \text{ hr}}$$

Thus

$$\frac{dV_m}{dt} = 7.29 \text{ ft}^3/\text{hr}$$

and therefore, the rate of melting would be

$$\frac{dM_i}{dt} = \rho_i \frac{dV_m}{dt}$$

where  $\rho_i$  is 56.7 lbm/ft<sup>3</sup>.

Using these values for the first 10 hours, the approximated rate of melting would be

$$\frac{dM_i}{dt} = (56.7)(7.29) = 413 \text{ lbm/hr.}$$

This approximate rate of melting is significantly greater than the average rate of 261 lbm/hr observed for the first 10-hr period (Table IV); in fact, it exceeds the observed rate by a factor of 1.6. The discrepancy, as stated previously, results from the simple assumption that the rate of change of the radius is constant.

While this method of approximation was acceptable when the rates of melting were unknown, an improved relationship can be developed to estimate the heat transfer coefficient now that the melting rates are available. Starting only with the assumptions that during the melting stage the ice remains in a cylindrical form and the melting occurs only in the radial direction, the rate of change of the radius as a function of the melting rate can be determined.

For a cylindrical geometry, the volume of the ice is given by

$$V_i(t) = \pi H_0 [R(t)]^2.$$

From this the volumetric rate of change of the ice is

$$\frac{dV_i}{dt} = 2\pi H_0 R(t) \frac{dR(t)}{dt}.$$

As in the previous approximation technique it will be assumed that the rate of change in the radius can be estimated by

$$\frac{dR}{dt} \approx \frac{\Delta R}{\Delta t}.$$

While presently the length of the period  $\Delta t$  is unspecified, it is obvious that as the length of this period decreases the accuracy of the approximation increases. At the limit as  $\Delta t$  approaches zero, it will be exact.

Therefore, the rate of change of volume is

$$\frac{dV_i}{dt} \approx 2\pi H_0 R(t) \frac{\Delta R}{\Delta t}.$$

Since this equation will be employed to approximate the rate of change during a specific time interval,  $t_1$  to  $t_2$ , a mean value for  $R(t)$  will be employed. Thus, if  $\Delta R$  is the decrease in the radius during the time interval from  $t_1$  to  $t_2$ , then the mean value of the radius during this interval is given by

$$R(t) = R(t_1) - \frac{\Delta R}{2}$$

where

$$t_1 < t < t_2$$

which upon substitution into the relationship for volume yields

$$\frac{dV_i}{dt} = 2\pi H_0 \left[ R(t_1) - \frac{\Delta R}{2} \right] \frac{\Delta R}{\Delta t}.$$

This expression is quadratic in terms of  $\Delta R$ . Solving for  $\Delta R$  in terms of the other variables yields

$$\Delta R = R(t_1) \pm \sqrt{R(t_1)^2 - \frac{\Delta t}{\pi H_0} \frac{dV_i}{dt}}.$$

Since  $R(t)$  must decrease in any interval from  $t_1$  to  $t_2$  and decrease from the initial value  $R_0$  to zero during the entire melting interval, the negative root must be used. Additionally, since

$$\frac{dV_i}{dt} = \frac{1}{\rho_i} \frac{dM_i}{dt}$$

then

$$\Delta R = R(t_1) - \sqrt{R(t_1)^2 - \frac{\Delta t}{\rho_i \pi H_0} \frac{dM_i}{dt}}. \quad (12)$$

From this relationship it is possible to determine the change in the radius of the ice cylinder during any time interval from  $t_1$  to  $t_2$ , provided that both the value of the radius at the beginning of the interval and the rate of melting during the interval are known.

To illustrate the improvement in the estimation of change in radius by using eq 12, Figure 19 has been

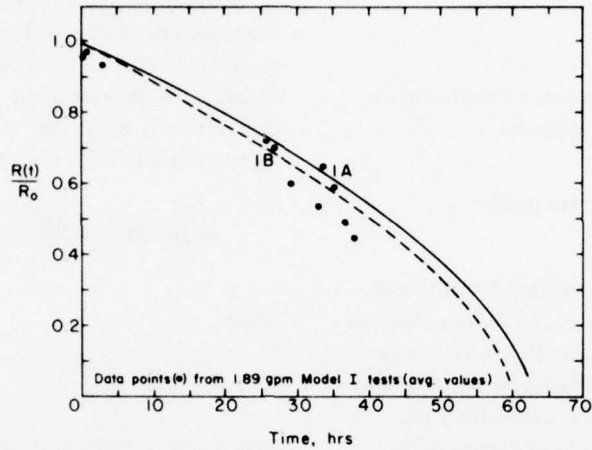


Figure 19. Approximated change in radius for Model II tests 1A and 1B.

Table XI. Approximation of the heat transfer coefficient, Model II, test 1B.

Time interval (hr)		$\bar{T}_i$ (°F)	$\bar{T}_o$ (°F)	$\bar{T}_b$ (°F)	$\Delta \bar{T}_m^*$ (°F)	$dM/dt^†$ (lbm/hr)	$R(t_1)$ (ft)	$\Delta R^{**}$ (ft)	$dR/dt$ (ft/hr)	$h^{\dagger\dagger}$ (Btu/hr ft <sup>2</sup> °F)
$t_1$	$t_2$									
0	10	54.2	37.7	46.0	14.0	286	3.0	0.34	0.034	19.90
10	20	55.9	38.4	47.1	15.1	264	2.66	0.36	0.036	19.44
20	30	56.1	37.8	46.9	14.9	227	2.30	0.36	0.036	19.69
30	40	57.1	39.3	48.2	16.2	205	1.94	0.40	0.040	20.18
40	50	58.2	40.5	49.4	17.4	191	1.54	0.50	0.050	23.53
50	60	63.7	46.5	55.1	23.1	161	1.04	0.97	0.097	34.20

\* From eq C2.

† From Table VIII.

\*\* From eq 12.

†† From eq C1.

developed with data from the two 4.73-gpm tests, tests 1A and 1B. Also included in this figure are radial measurements taken at various stages of melting of the ice cylinder from the two 1.89-gpm Model I tests. The measurements, which were made at  $\frac{1}{3}$  and  $\frac{2}{3}$  of the tank elevation in the Model I tests, have been averaged to give an overall change in radius. A comparable time basis between the Model I and Model II tests was developed by using the scaling factor as discussed in Appendix B. All values of the radius have been normalized by division by the initial radius values, 3.0 ft for Model II and 2.0 ft for Model I.

As illustrated in Figure 19 there is a high degree of correlation between the approximated values and the measured average values. In general the correlation is best during the early melting stages; the largest deviations occur during the final hours. The decrease in accuracy of the approximated solution is to be expected, since as melting proceeds, the discrepancy increases between the assumed and actual melting geometry. Although errors tend to be greater during the final hours, this revised approximation technique represents a substantial improvement over the earlier method.

This method of approximation also results in a distinct improvement in the estimation of the heat transfer coefficient. Not only can the term  $\Delta R/\Delta t$  in eq 9 be approximated with a higher degree of accuracy, it is possible to estimate the heat transfer coefficient during different time intervals within a particular test.

As with the earlier approximation there are, however, definite limitations on the application of these equations. The most basic limitation results from variations between the assumed and actual melting geometry. In the model sink the rate of change of the radius is not only a function of time but also of the height of the ice cylinder. Additionally, melting occurs on the upper and lower horizontal surfaces. Even if these other effects were included, some allowance would also need to be made for the point of introduction or melt scour patterns associated with the inlet header manifold arrangement.

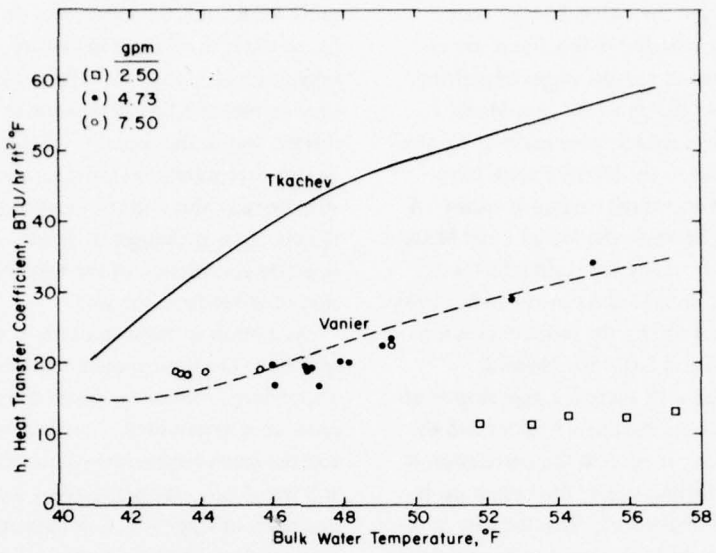
Although not readily apparent, there is another implied limitation in these equations. While the accuracy of the approximation will generally increase as the length of the time interval  $\Delta t$  is decreased, there is a lower boundary on the minimum size of this interval. Since the equations depend upon the determination of the melting rate which itself is calculated by detectable changes in volume, they can only be employed for

fairly significant time intervals. In the conversion of ice to water the change in density, and thus volume, is only approximately 9%. Theoretically, it would be possible to measure this change for as little as 10 lb of ice melted, but in the actual test apparatus, a much larger change is required to ensure reasonable measurements. Additionally this is also influenced by second order effects, such as changes in density of the water, expansion and contraction of the test apparatus and evaporation of water from the sink.

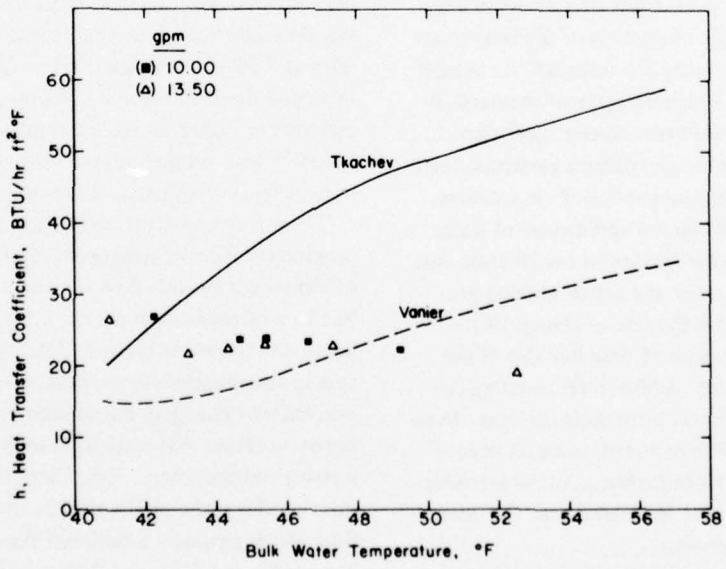
As a result of these limitations the approximation technique has been applied to 10-hour intervals corresponding to those for which the average melting rates were determined. In using these 10-hour intervals the mean temperature difference between the ice and water  $\Delta T_m$  is calculated by using the procedure described in Appendix C as applied to the specific time interval. A sample calculation of the heat transfer coefficients for test 1B is illustrated in Table XI. The approximated heat transfer coefficients for all the Model II tests appear on Figures 20a and 20b, where the variations have been plotted vs the calculated bulk water temperature. These results have been divided into two flow rate-related regimes: a low flow rate zone depicting relationships for flow rates of 7.50-gpm and less, and a high flow rate zone depicting the 10.00- and 13.50-gpm test results. Also included in Figure 20 are the results of Tkachev<sup>16</sup> and Vanier<sup>18</sup> who studied, respectively, turbulent and natural free convective melting of ice.

There is an excellent correlation between the approximated heat transfer coefficients and the results of Vanier for the test flow rates of 4.73 and 7.50 gpm. The lack of correlation for the 2.50-gpm tests is believed due to two influences. For this test, melting occurs in a predominantly vertical rather than radial manner, thereby changing the surface area over which melting occurs from that associated with the assumed radial melting configuration. The other effect influencing this variance is the predominance of the density-related flow which produces a different flow pattern from that observed in the 4.73- and 7.50-gpm tests.

As flow rates were increased to 10.00 and 13.50 gpm a different trend became apparent. Unlike the low flow rate results which indicated a gradual increase in heat transfer coefficient, it appears that for these two tests the heat transfer coefficient becomes approximately constant. Additionally, since as the heat test proceeds,



a. For low flow rates.



b. For high flow rates.

Figure 20. Heat transfer coefficients for Model II.

the bulk water temperature generally increases (see Table XI), these higher flow rate results tend to proceed from a correlation with the results of Tkachev<sup>16</sup> to a correlation with the results of Vanier.<sup>18</sup> This in turn would indicate a possible transition in flow behavior from "pseudo-turbulent" free convection to "pseudo-natural" free convection. The use of the prefix "pseudo" should be noted, since in all the tests there is an imposed overall forced flow condition; that is, water is added at the top of the sink at a specific rate and removed from the bottom at the same rate. Of course, this does not actually require that the water "flow" through the sink, since in the lowest flow rate tests it was observed that "flow" was actually the motion of a horizontally stratified layer through the test tank.

To examine possible correlations of the heat transfer coefficient and coolant water flow rate, the approximated heat transfer coefficients have been plotted versus a Reynolds number based on an equivalent diameter (see App. C) in Figure 21. They have also been tabulated in Table XIIa for test flow rates of 4.73 gpm and less and in Table XIIb for flow rates of 7.50 gpm and greater. As indicated in the figure, two distinct trends can be discerned. For the test flows of 2.50 and 4.73 gpm there appears to be a significant change in heat transfer coefficient with changes in Reynolds number. Unlike the behavior indicated in Figure 20a, the results of the 2.50-gpm test appear to correlate with the others on a flow rate basis. Another difference with the trends indicated in Figure 20a is that the 7.50-gpm test results do not indicate any correlation with the results of the 4.73-gpm tests; rather, they indicate a transition between the results obtained with the lower and higher flow rate tests. Again, the results of the highest flow rate tests indicate that the heat transfer coefficient tends to approach a constant value over the range of Reynolds numbers applicable to the experimental tests.

The trends illustrated in Figures 20 and 21 tend to indicate that some form of correlation exists which can be used to relate the heat transfer coefficient to the applicable test conditions. The most general form would be a relationship involving the Nusselt number as a function of other dimensionless parameters. Before discussing these relationships some background information might be useful.

In general two basic correlations can be established, as illustrated by Figures 20 and 21. The first would be

Table XII. Heat transfer coefficient for various Reynolds numbers.

Test no.	Reynolds number ( $Re_{DE}$ )	Heat transfer coefficient $h$ (Btu/hr ft <sup>2</sup> °F)
<b>a. For 2.50- and 4.73-gpm tests</b>		
2	44.0	11.6
2	47.4	11.5
2	51.1	12.4
2	56.1	12.3
2	62.2	13.2
1A	75.9	16.8
1B	76.0	19.9
1A	81.8	17.0
1B	82.4	19.4
1A	86.4	19.0
1B	87.9	19.7
1A	94.7	20.5
1B	97.1	20.2
1A	106.0	22.5
1B	109.5	23.5
1A	130.3	29.1
1B	145.7	34.2
<b>b. For 7.50-, 10.00- and 13.50-gpm tests</b>		
4	114.7	18.5
4	120.4	18.3
4	125.6	18.8
4	133.9	18.9
4	146.2	19.1
3	151.0	27.1
3	167.5	23.7
4	170.1	22.6
3	181.9	23.8
5	198.9	26.3
3	202.0	23.4
5	217.2	21.9
3	233.6	22.3
5	234.5	22.5
5	256.4	23.2
5	289.1	23.0
5	350.7	19.1

typical of a natural convective problem, the variations in heat transfer coefficient and thus Nusselt number resulting directly from temperature-density induced influences. In parametric form this is typically expressed as

$$Nu = f_1(Gr Pr)$$

where Gr and Pr represent the Grashof and Prandtl numbers, respectively. On the other hand the results of Figure 21 indicate a different form of correlation, specifically:

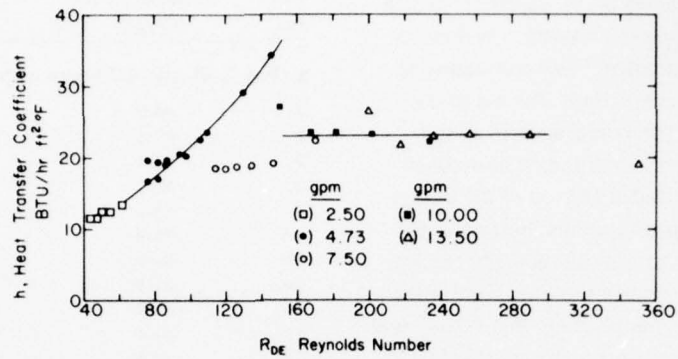


Figure 21. Heat transfer coefficient vs Reynolds number, Model II.

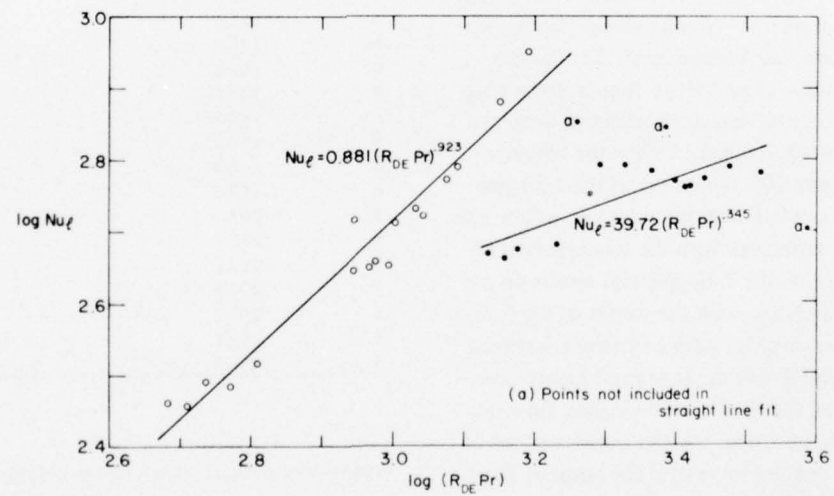


Figure 22. Variation in Nusselt number with Reynolds number, Model II.

$$Nu = f_2(Re \ Pr)$$

where  $Re$  is the Reynolds number. The questions which arise pertain to the parametric form which would best result in predicting the dominant influence and the variables which should be selected as the characteristic dimensions needed to nondimensionalize the parameters. If a relationship of the  $(Gr \ Pr)$  type is assumed, normal practice dictates the use of the length of the ice cylinder as the characteristic dimension. If the  $(Re \ Pr)$  form is selected, correlations are generally based on the use of some type of diameter; however, there are instances where a length factor has been included.

In the selection of the parameters it was decided to use a relationship of the  $(Re \ Pr)$  type with a Reynolds number based on an equivalent diameter and a Nusselt number based on the length of the ice cylinder. The use of an equivalent diameter for correlating flows in annular passages is fairly common;<sup>4</sup> however, only relationships concerning forced convection could be found in the literature. The use of length in the calculation of the Nusselt number for correlation with Reynolds number based on a diameter is somewhat of a break with traditional approaches but was selected for two specific reasons.

The first reason is a rather practical one. If the equivalent diameter is selected as the characteristic dimension for the Nusselt number, it produces extremely large variations in the calculated values. For example, when an equivalent diameter is used in test 1A the average Nusselt number for the first 10-hour period would be only 14.2. On the other hand for the last 10-hour period it would be 384.9. Thus for a 73% increase in the heat transfer coefficient, from 16.8 to 29.1 (see Table XIIa), the Nusselt number would increase by approximately 2710%. This does not appear to be a very reasonable method on which to base a correlation. If instead, the length of the ice cylinder is employed, the 73% increase in heat transfer coefficient results in the same proportional increase in Nusselt number. Here the characteristic length is assumed to remain constant at the initial length, which is consistent with the assumptions used in the derivation of the approximation equations for the heat transfer coefficient.

The second, and more fundamental, reason is illustrated by examining the relationship between free and forced convection. Free convection can be considered

to be the limiting case of forced convection when influences of the Reynolds number type can be neglected. As indicated by Table XII and Figure 21, the Reynolds numbers for the Model II tests are indeed small and tend to approach the zone wherein they would have no effect at all. As stated previously for the lowest flow rate tests, density (i.e. free convective) related influences predominate even under the imposed forced flow conditions. Thus over the range of flow rates tested, the Model II heat sink apparently is influenced by both density and flow velocity parameters. Since the normal correlation of free convection of vertical cylinders employs the characteristic length of the cylinder as the characteristic dimension, it was felt appropriate to also use this dimension in calculating Nusselt numbers.

The results of this analysis are presented in Figure 22. As in Figure 21 there are two distinct zones, the first applicable to flow rates of 4.73 gpm and less and the second to flows of 7.50 gpm and greater. Again there is some overlap between the two zones, indicating some transitional effects. This correlates with the observed transition in the behavior of the outlet water *after melting that occurred within this same range of flow rates*. Using a least squares fit for the two different sections, the following relationships have been developed:

$$Nu_q = 0.881(Re_{DE} \ Pr)^{0.923} \quad (13a)$$

for

$$450 < Re_{DE} \ Pr < 1400$$

and

$$Nu_q = 39.72(Re_{DE} \ Pr)^{0.345} \quad (13b)$$

for

$$1400 < Re_{DE} \ Pr < 3500.$$

In the section of this report which compared the results of the two different models, there appeared to be a deviation between the linear flow rate scaling relationships postulated in Appendix B and the observed average outlet water temperatures, as illustrated in Figure 11. It was noted that a better correlation between the outlet water temperatures for the two models would occur if the flow rate zone from 3.0 to 4.0 gpm in

Model I were shifted to correspond to the Model II range from 4.75 to 7.5 gpm rather than the linearly scaled range of 7.5 to 10.0 gpm. By assuming various ice diameters for these Model I and Model II tests and comparing Reynolds numbers, it is possible to explain the probable reason for this nonlinearity in scaling. As the diameter of the ice cylinder decreased from 3.5 ft to 0.5 ft in the 3.00-gpm Model I test (nominal tank diameter was 4.0 ft), the Reynolds number (based on an equivalent diameter) varied from 77.5 to 129. For the 4.00-gpm Model I test the same changes in diameter resulted in a variation in Reynolds number between 98 and 164. In the Model II test with a flow rate of 4.73 gpm the variation in Reynolds number is between 76 and 130. This would indicate that on a flow rate basis a more comparable flow relationship exists between the 3.00-gpm Model I and 4.73-gpm Model II tests rather than the linearly scaled 3.00-gpm Model I and 7.50-gpm Model II experiments. Similarly the variation in Reynolds number from 98 to 164 for the 4.00-gpm Model I test closely corresponds to the 7.50-gpm Model test which had a Reynolds number variation from 115 to 170. Although this analysis indicates the limitations of the linear scaling relationships, they are extremely useful for quickly estimating heat loads and flow rates. However, once these initial parameters have been estimated, an analysis of the Reynolds number type would be more appropriate for establishing practical operational parameters.

Of course equations 13a and 13b cannot represent a complete characterization of the melting process. As stated earlier there are density-related effects which undoubtedly should be included, possibly by means of a Grashof number term. Without considerable data available at a constant Reynolds number, it is impossible to define this functional relationship; however, for the lower flow rate zone (i.e.  $Re_{DE} Pr$  less than 1400), it appeared that increases in the Grashof number resulted in small decreases in the heat transfer coefficient. This is reasonable if the density-related effects (upward) are opposed to the normal flow direction (downward). It is important to recognize that while the relationships developed in this report used certain parameters and characteristic dimensions, other satisfactory correlations are quite possible. It is felt that other variables such as the aspect ratio of the ice, i.e. the length to diameter ratio, could also be important. Due to the limited scope of this study and

the generalized nature of the calculations, a more detailed analysis is not possible.

## CONCLUSIONS AND RECOMMENDATIONS

A major concern recognized during previous experimental studies with ice-water heat sinks was the potential problem in scaling results from the small model to a prototype having a volume approximately 5000 times larger. The experimental results reported herein were obtained on a heat sink which was 3.75 times larger volumetrically than the original model. This report has presented 1) the experimental results of using the larger model, 2) a comparison of these results with those predicted by a previously developed computer program and 3) a comparison of results from the two scale model test series.

Over the range of flow rates tested, it was found that a rather well-defined transition developed in the pattern of water flow through the sink. At the lowest flow rates, distinct water layers formed which were essentially isothermal and melting progressed primarily from the top downward, rather than radially inward from the annular space around the ice cylinder. At the highest flow rates, the dominant melting mode was radial and the flow is rather well-mixed. At the intermediate flow rates the melt pattern represents a balance between mixed and stratified flow.

Except for some anomalous behavior at the intermediate flow rates, the average outlet water temperature during the melting period tended to increase as flow rate increased. For both the model studies this average value varied between about 36°F and 44°F; subsequent to melting the sink outlet temperature increases rapidly. The coolant water flow rate did not appear to significantly influence the rate of melting, particularly during the last half of the melting period (Fig. 13). During the early stages of melting the influence of water flow rate tended to be masked by other factors, such as a difference in the average ice temperature at the start of the test.

A comparison between computer predictions and experimental measurement was made on the basis of 1) mean outlet temperature during the melting period, 2) overall time required to complete melting, and 3) behavior of the outlet water temperature after all the ice is melted. The computer solutions for outlet water temperatures during average melting periods tended to

predict a slightly higher temperature than was actually measured by about 1° to 3°F in most cases (Fig. 11); this is felt to represent a satisfactory prediction, and the overestimation of temperature tends to be slightly conservative. Also, as presently structured, the computer program fails to simulate the temperature stratification phenomenon observed subsequent to melting in the lowest flow rate experiment. Rather, the program predicts a slight plateau in outlet temperature which is more representative of the higher flow rate tests. This limitation is not felt to be a serious drawback, and a simple relationship is presented in this report to more accurately depict this temperature-time relationship.

It appears that the computer predictions could be used to design a prototype sink whose actual outlet water temperature will be generally lower than that predicted. The small error in the prediction could be considered to be a slight safety factor in the selection and sizing of a prototype system. The computer program did predict the melting times rather accurately (Table VII).

The scaling relationships presented in Appendix B appear to provide a reasonable method for comparing the results of the two model heat sinks of different size. At present there appears to be no reason to doubt the use of these scaling relationships to estimate possible heat rejection and coolant water flow rates in a prototype installation. In those flow rate regions where good correlation between the models was not obtained using these scaling relationships, a method was developed to account for nonlinearities. It is recommended that the relationships of Appendix B should be employed to determine initial values in the sizing of a prototype sink, and that these values should be refined by the techniques described in the section of this report which discussed the approximation of the heat transfer coefficient. Based on the small number of tests conducted during these programs, it is believed that the overall results indicate the general applicability of the scaling relationships to approximate the behavior of any size heat sink used in a similar manner, giving due consideration to the nonlinear effects indicated by the Reynolds number analysis.

By using a simplified radial melting mathematical model, variations in gross average heat transfer coefficients were obtained. When the heat transfer coefficient was calculated for 10-hour intervals, the results

were found to correlate quite well for the lower flow rate tests with values determined by Vanier<sup>18</sup> who studied natural laminar convective melting of ice oriented in a vertical plane. Heat transfer coefficients were correlated with the flow conditions by using a Nusselt number based on the height of the ice and a Reynolds number based on an equivalent diameter of the annular space between the ice and the heat sink tank. The correlation indicated that two distinct zones exist, one for test flow rates of 4.73 gpm or less and the other for flows of 7.50 gpm or greater. The transition between the zones appears to occur when the Reynolds number during the initial hours of melting lies in the range of 100 to 120. The two relationships developed were

$$Nu_q = 0.881(Re_{DE} Pr)^{0.923}$$

for

$$450 < (Re_{DE} Pr) < 1400$$

and

$$Nu_q = 39.72(Re_{DE} Pr)^{0.345}$$

for

$$1400 < (Re_{DE} Pr) < 3500.$$

The Reynolds number analysis was also found to be useful in explaining the nonlinearities that occurred when using the flow rate scaling procedures of Appendix B.

Within reasonable limits of accuracy, the computer program does simulate the behavior of the heat sink and can be employed as a basis of design for a prototype sink. The use of the computer program as a design basis, rather than the scaling of the experimental results, is recommended since a prototype installation would employ both variable coolant flow rates and heat rejection rates — conditions that are easily accommodated using the computer model.

From the results of the experimental tests conducted using the Model I and Model II heat sinks, it is recommended that future work should primarily be concerned with the investigation of alternative inlet/outlet header configurations and the behavior of the sink at high coolant water flow rates. The use of a

spray type inlet header in a limited number of Model I tests resulted in the creation of very favorable conditions and could result in an improvement in the efficiency of the power plant/heat sink system. It is felt to be important to analyze the effects of this and other proposed configurations prior to the construction of a prototype sink.

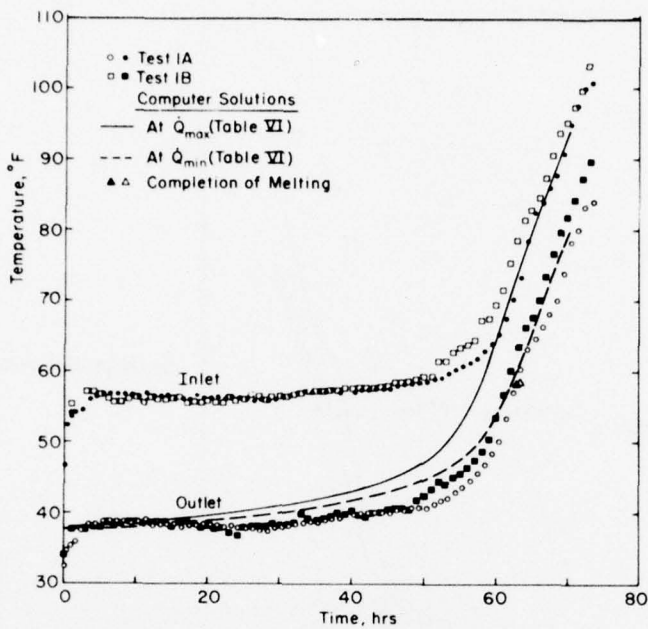
The tendency of the sink to provide a constant average outlet water temperature during the melting period in the higher flow rate tests also appears to merit further investigation. Should this trend continue, extremely simple relationships can be developed to accurately predict the behavior of the sink at these higher flow rate levels.

While mentioned only briefly in this report, the authors would like to emphasize that to date little information can be found in the literature concerning the heat and mass transfer at an ice/water interface under conditions similar to those which occur in the heat sink.

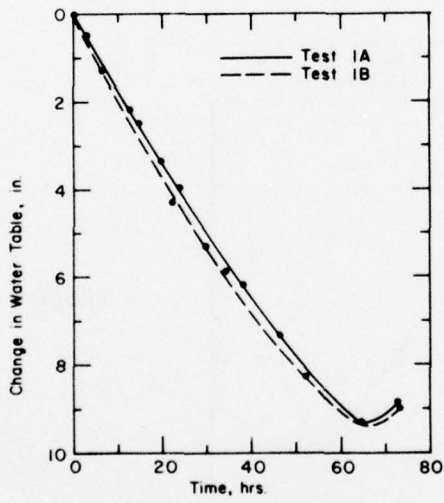
## LITERATURE CITED

1. Baumeister, T. and L.S. Marks (1967) *Standard handbook for mechanical engineers*. New York: McGraw-Hill, Inc.
2. Becker, E. and J.L. Brown (1970) An investigation of a multiple hole ice-water heat sink. U.S. Army Cold Regions Research and Engineering Laboratory (USA CRREL) Technical Note (unpublished).
3. Brown, J.L. and W.F. Quinn (1975) An annular flow ice-water model heat sink study. CRREL Special Report 236. AD A015468.
4. Chapman, A.J. (1967) *Heat transfer*. New York: MacMillan Company.
5. Dill, R.S. and A.B. Peavy (1956) Some observations on the use of underground reservoirs as heat sinks. National Bureau of Standards Report 4795.
6. Garg, S.C. (1973) Earth heat sinks for underground power sources. Naval Civil Engineering Laboratory Technical Note N-1306.
7. Grande, E. (1975) Analysis and conceptual design of a practical ice-water heat sink. CRREL Special Report 221. AD A009498.
8. Greenberg, M. (1973) Chronological review of heat sink studies. U.S. Army Engineer Power Group, Ft. Belvoir, Virginia.
9. Hubbard, F.R. III (1967) Tunnel condenser concept (U). Nuclear Power Field Office, Ft. Belvoir, Virginia. (CONFIDENTIAL)
10. Parson, Brinckenhoff, Hall and MacDonald (1958) Feasibility study - icing of underground reservoirs (U). (SECRET)
11. Perham, R.E. (1973) Model ice heat sink. CRREL Special Report 185.
12. Quinn, W.F. and M. Greenberg (1967) A study of the steam heat sink concept. CRREL Draft Report. (SECRET)
13. Quinn, W.F., H.W.C. Aamot and M. Greenberg (1971) Analysis and test of a rock-steam condenser heat sink concept. Winter Annual Meeting of the American Society of Mechanical Engineers on Environmental and Geophysical Heat Transfer, Heat Transfer Division, vol. 4, p. 70-77.
14. Stubstad, J. and W.F. Quinn (1974) Experimental study of several ice heat sink concepts. CRREL Special Report 208. AD 782942.
15. Tien, C. (1960) Analysis of a sub-ice heat sink for cooling power plants. U.S. Army Snow, Ice and Permafrost Research Establishment (USA SIPRE) Research Report 60. AD 696399.
16. Tkachev, A.G. (1953) Experimental investigation of heat exchange in melting. U.S. Atomic Energy Commission Translation Series TR-3405, p. 169-178.
17. USA CRREL (1966) Studies of underground heat sink concept (U). CRREL Draft Report (CONFIDENTIAL)
18. Vanier, C.R. (1967) Free convection melting of ice. Syracuse University M.S. thesis (unpublished).
19. Zehnder, A., Y.C. Yen, R. Perham and W.F. Quinn (1973) An analytical study of a coiled pipe heat sink. CRREL Special Report 195. AD 771125.

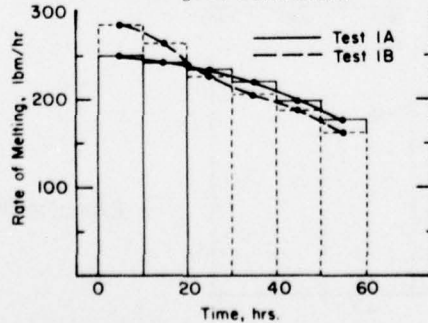
## APPENDIX A: EXPERIMENTAL DATA, HEAT SINK MODEL II



a. Inlet and outlet water temperatures.

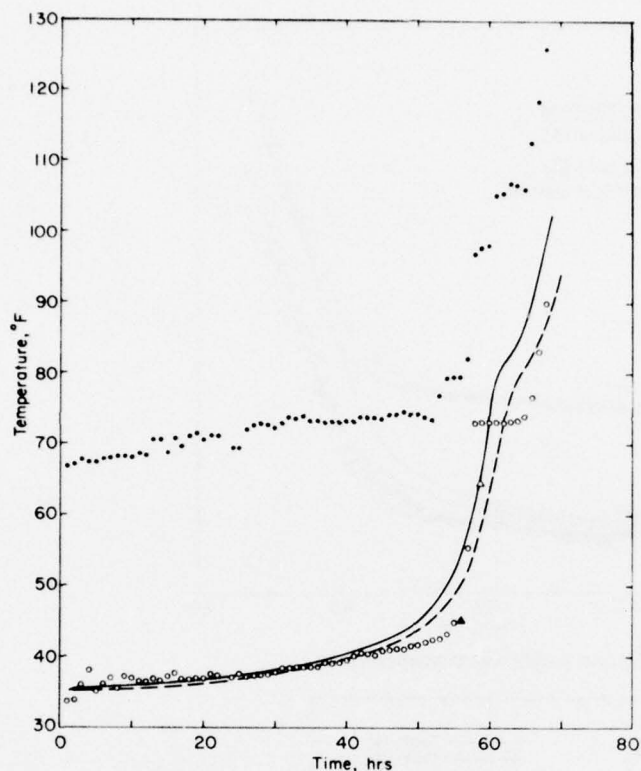


b. Change in water table.

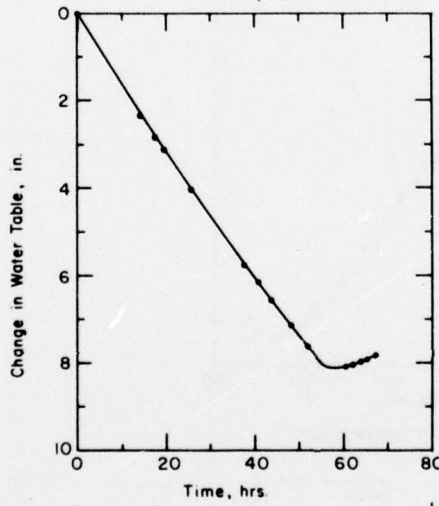


c. Rate of melting.

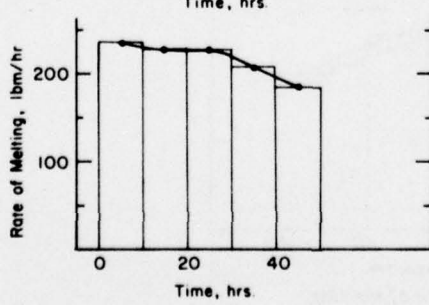
Figure A1. Temperature-time and rate of melting curves for the 4.73-gpm tests.



a. Inlet and outlet water temperatures.

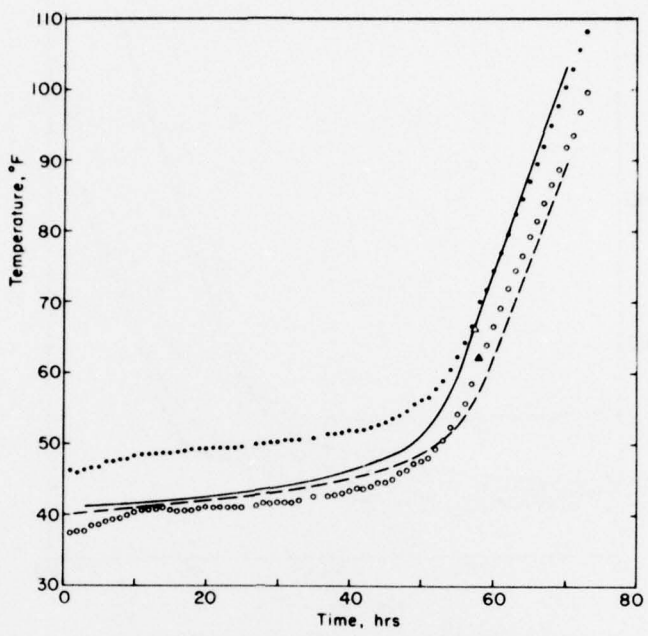


b. Change in water table.

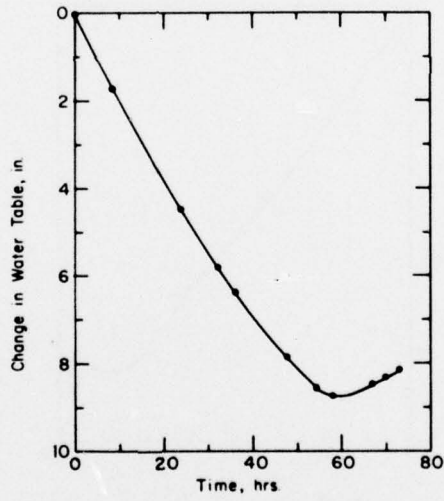


c. Rate of melting.

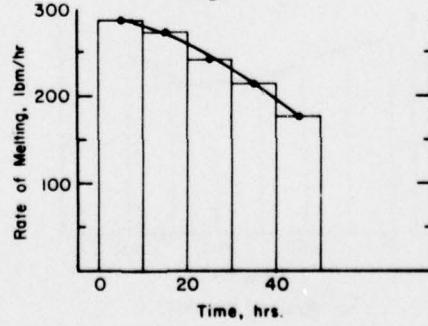
Figure A2. Temperature-time and rate of melting curves for the 2.50-gpm test.



a. Inlet and outlet water temperatures.

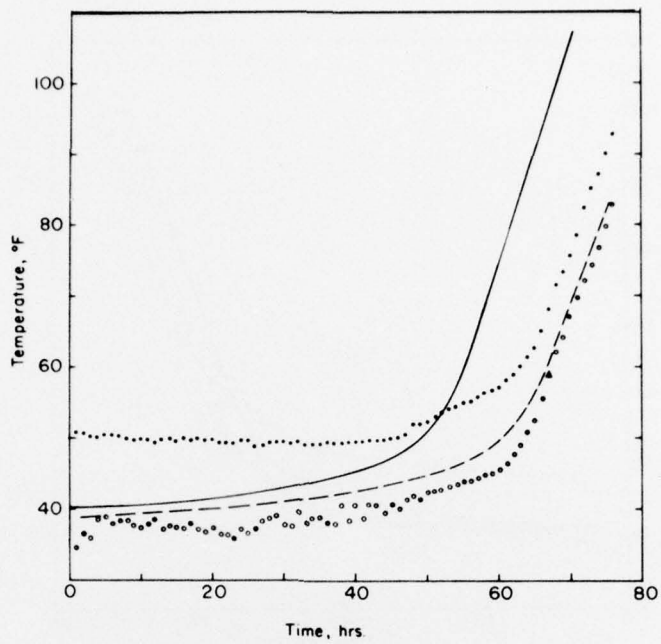


b. Change in water table.

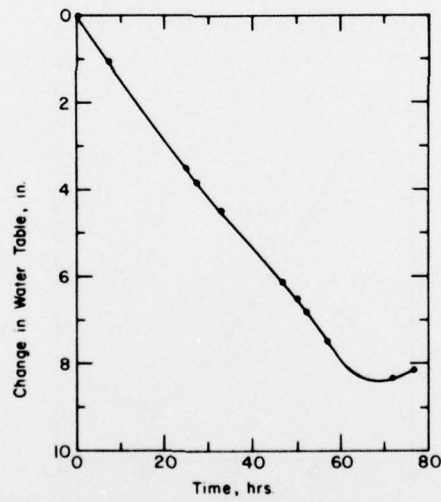


c. Rate of melting.

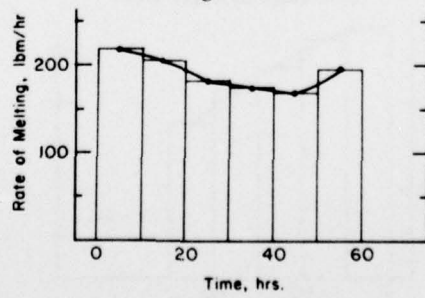
Figure A3. Temperature-time and rate of melting curves for the 10.00-gpm test.



a. Inlet and outlet water temperatures.

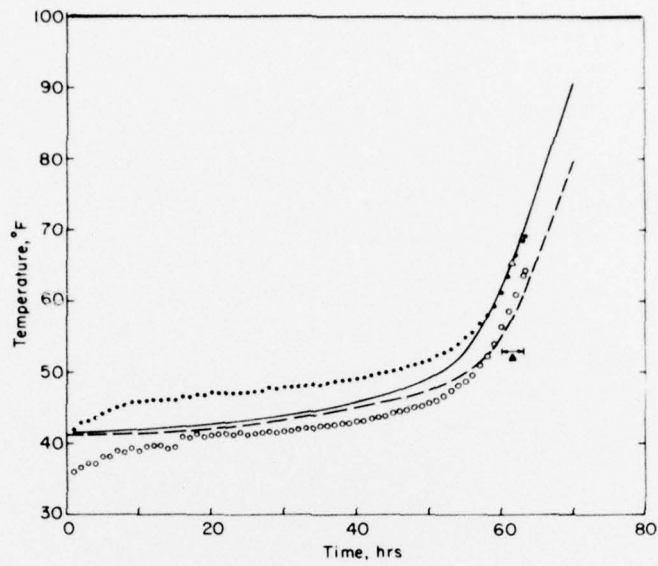


b. Change in water table.

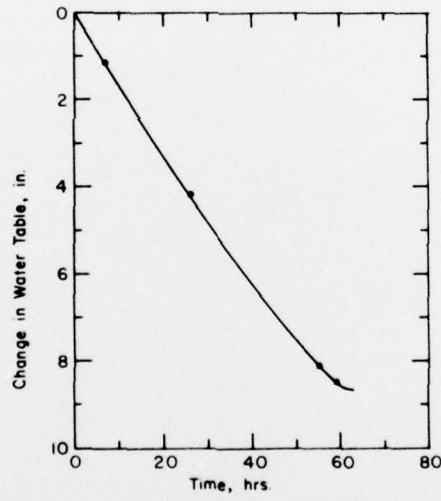


c. Rate of melting.

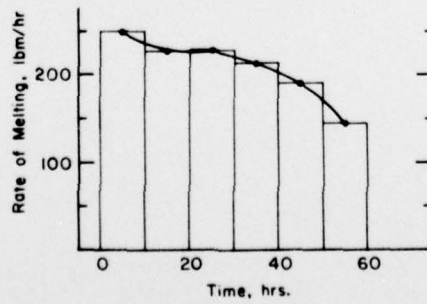
Figure A4. Temperature-time and rate of melting curves for the 7.50-gpm test.



*a. Inlet and outlet water temperatures.*



*b. Change in water table.*



*c. Rate of melting.*

*Figure A5. Temperature-time and rate of melting curves for the 13.50-gpm test.*

## APPENDIX B: HEAT SINK SCALING AND SIMILARITY RELATIONSHIPS

(From Brown and Quinn<sup>3</sup>)

### Dimensional scaling

The dimensional scaling is relatively straightforward. Quite simply for the prototype and model to be comparable:

$$(R_0/L)_{\text{model}} = (R_0/L)_{\text{proto}} \quad (\text{B1})$$

$$(R/R_0)_{\text{model}} = (R/R_0)_{\text{proto}} \quad (\text{B2})$$

where  $R_0$  = the initial radius of the ice cylinder  
 $R$  = the radius at comparable times  
 $L$  = the initial length of the ice cylinder.

### Temperature scaling

Heat is transferred to the ice by natural convection which, particularly for water, is highly dependent on both temperature difference and absolute temperature. This dependence is due to the density-temperature relationship of water which exhibits a maximum value at 4°C. Since the heat transfer process is so highly dependent on temperature, the temperatures of the model and the prototype must be directly equivalent. Thus,

$$T_{\text{model}} = T_{\text{proto}}$$

and

$$\Delta T_{\text{model}} = \Delta T_{\text{proto}}$$

### Heat transfer scaling

For the heat transfer phenomena in the model to be comparable to those of the prototype, the relative effects of the various modes of heat transfer and storage must be equated. In this particular study, heat is absorbed in the heat sink by two methods: 1) heating of the water in the sink  $Q_w$ , and 2) melting of the ice, thereby utilizing its latent heat  $Q_m$ .

Thus, the total heat rejected to the sink  $Q_R$  up to a given point in time is

$$Q_R = Q_m + Q_w$$

This allows for the formulation of a "heat storage" parameter:

$$N_s = \frac{Q_m}{Q_R}$$

And for the prototype and model to be comparable

$$(N_s)_{\text{model}} = (N_s)_{\text{proto}}$$

We have a requirement that the heat rejection rates must be related. Thus, the percentage of heat rejected through melting must be comparable for the model and prototype. Thus,

$$N_s = \frac{\dot{Q}_m}{\dot{Q}_R}$$

$$\left( \frac{\dot{Q}_m}{\dot{Q}_R} \right)_{\text{model}} = \left( \frac{\dot{Q}_m}{\dot{Q}_R} \right)_{\text{proto}}$$

or

$$\frac{\dot{Q}_{m(\text{model})}}{\dot{Q}_{m(\text{proto})}} = \frac{\dot{Q}_{R(\text{model})}}{\dot{Q}_{R(\text{proto})}}$$

Now

$$\dot{Q}_m = h_{\text{conv}} A \Delta T$$

$$= h_{\text{conv}} A (T_B - 32)$$

where  $h_{\text{conv}}$  = convective heat transfer coefficient

$A$  = surface area of ice

$T_B$  = bulk water temperature.

Thus

$$\frac{\dot{Q}_{R(\text{model})}}{\dot{Q}_{R(\text{proto})}} = \frac{(h_{\text{conv}} A \Delta T)_{\text{model}}}{(h_{\text{conv}} A \Delta T)_{\text{proto}}}$$

As noted above, the temperatures must remain equivalent, thus

$$\frac{\dot{Q}_{R(\text{model})}}{\dot{Q}_{R(\text{proto})}} = \frac{(h_{\text{conv}} A)_{\text{model}}}{(h_{\text{conv}} A)_{\text{proto}}} = \frac{(h_{\text{conv}} R_0 L)_{\text{model}}}{(h_{\text{conv}} R_0 L)_{\text{proto}}}$$

For turbulent flow,  $h_{\text{conv}}$  is independent of size; thus

$$h_{\text{conv(model)}} \approx h_{\text{conv(proto)}}.$$

These scaling relationships can now be summarized.

For the general case:

$$\frac{\dot{Q}_{R(\text{model})}}{\dot{Q}_{R(\text{proto})}} = \frac{(h_{\text{conv}} A)_{\text{model}}}{(h_{\text{conv}} A)_{\text{proto}}} \quad (\text{B3})$$

For the turbulent case:

$$\frac{\dot{Q}_{R(\text{model})}}{\dot{Q}_{R(\text{proto})}} = \frac{A_{\text{model}}}{A_{\text{proto}}} \quad (\text{B4})$$

where  $A = 2\pi R_0 L$ . A means for scaling the time factor must now be derived. For this case, the percentage of total heat absorbed must be equal for equivalently scaled times. Thus

$$\frac{Q_R}{Q_{TC}} = \int \frac{\dot{Q} d\theta}{Q_{TC}}$$

where  $Q_{TC}$  is the total heat-absorbing capacity of the heat sink system.

Assuming that heat is rejected at a constant rate, the coolant water flows at constant volume, and the initial sink consists solely of ice, the following relationship holds:

$$\frac{Q_R}{Q_{TC}} = N_q = M_{\text{sink}} \frac{W C_p \theta \Delta T}{(H + C_p \Delta T_{\text{max}})}$$

where  $\Delta T$  = constant temperature difference across the sink,  $T_{\text{in}} - T_{\text{out}}$

$\Delta T_{\text{max}}$  = maximum allowable sink temperature,

$T_{\text{max}} - 32^{\circ}\text{F}$

$W$  = mass flow rate, lbm/hr

$C_p$  = specific heat of water, 1.0 Btu/lbm  $^{\circ}\text{F}$

$M_{\text{sink}}$  = mass, lb

$H$  = latent heat of fusion, 144 Btu/lbm

$\theta$  = time, hr.

For comparable cases (of model vs prototype) the temperature  $\Delta T$  and  $T_{\text{max}}$  are equal. Thus, since

$$(N_S)_{\text{model}} = (N_S)_{\text{proto}}$$

we may obtain

$$\left( \frac{W\theta}{M_{\text{sink}}} \right)_{\text{model}} = \left( \frac{W\theta}{M_{\text{sink}}} \right)_{\text{proto}} \quad (\text{B7})$$

We note that this is the same result as would be obtained by considering that the percentage of total mass circulated through the sink at equivalent times must be comparable. Thus

$$\left[ \frac{\theta}{(M_{\text{sink}}/W)} \right]_{\text{model}} = \left[ \frac{\theta}{(M_{\text{sink}}/W)} \right]_{\text{proto}} \quad (\text{B6})$$

It should be noted that this result is also obtainable from the "storage" parameter:

$$N_s = \frac{\dot{Q}_m}{\dot{Q}_R}$$

$$\text{where } \dot{Q}_m = (2\pi r L) \rho H \dot{r}$$

$\rho$  = density of ice, lbm/ft<sup>3</sup>

$$\dot{r} = dr/d\theta.$$

Thus

$$N_s = \frac{(2\pi r L) \rho H \frac{dr}{d\theta}}{W C_p \Delta T}.$$

For the model and prototype to be considered equivalent

$$N_{s(\text{model})} = N_{s(\text{proto})}.$$

Thus, eliminating equivalent terms,

$$\left( \frac{L R \dot{R}}{W} \right)_{\text{model}} = \left( \frac{L R \dot{R}}{W} \right)_{\text{proto}}$$

where  $\dot{R}$  is the instantaneous radius at time  $\theta$ . Now consider

$$\dot{r} = \frac{dR}{d\theta}.$$

It is essential that a dimensionless time factor be formed if equivalent time scaling is to exist:

$$\left(\frac{\theta}{\theta^*}\right)_{\text{model}} = \left(\frac{\theta}{\theta^*}\right)_{\text{proto}}$$

where  $\theta^*$  is time in which all ice will be melted and sink water is brought to its maximum allowable temperature  $T_{\max}$ , and

$$\theta^* = \frac{M_{\text{sink}}(H + C_p T_{\max})}{\dot{Q}_R}$$

Thus

$$\dot{r} = \frac{r_0}{\theta^*} \frac{d(R/R_0)}{d(\theta/\theta^*)}$$

where  $R_0$  is the initial ice cylinder radius. Now

$$(R/R_0)_{\text{model}} = (R/R_0)_{\text{proto}}$$

when

$$(\theta/\theta^*)_{\text{model}} = (\theta/\theta^*)_{\text{proto}}$$

Thus

$$\left[ \frac{d(R/R_0)}{d(\theta/\theta^*)} \right]_{\text{model}} = \left[ \frac{d(R/R_0)}{d(\theta/\theta^*)} \right]_{\text{proto}}$$

This result is used in obtaining

$$\begin{aligned} \frac{1}{W} \left[ L \left( \frac{R}{R_0} R_0 \right) \left( \frac{R_0}{\theta^*} \right) \frac{d(R/R_0)}{d(\theta/\theta^*)} \right]_{\text{model}} &= \\ &= \frac{1}{W} \left[ L \left( \frac{R}{R_0} R_0 \right) \left( \frac{R_0}{\theta^*} \right) \frac{d(R/R_0)}{d(\theta/\theta^*)} \right]_{\text{proto}}. \end{aligned}$$

Cancelling equivalent terms

$$\left( \frac{LR_0^2}{W\theta^*} \right)_{\text{model}} = \left( \frac{LR_0^2}{W\theta^*} \right)_{\text{proto}}$$

which becomes the same result as obtained above when inverted and multiplied by  $\pi \rho_{\text{ice}}$ :

$$\left( \frac{W\theta^*}{M} \right)_{\text{model}} = \left( \frac{W\theta^*}{M} \right)_{\text{proto}}$$

### Summary of dimensional and heat transfer similarities

Based upon the above discussion when the following series of requirements are followed, the scale model and prototype are comparable:

1. Temperature scaling:

$$\Delta T_{\text{model}} = \Delta T_{\text{proto}}$$

$$\Delta T = T_{\text{in}} - T_{\text{out}}$$

$$T_{\text{model}} = T_{\text{proto}}$$

2. Dimensional scaling:

$$(R/R_0)_{\text{model}} = (R/R_0)_{\text{proto}}$$

and

$$(R_0/L)_{\text{model}} = (R_0/L)_{\text{proto}}$$

3. Time scaling:

$$(\theta/\theta^*)_{\text{model}} = (\theta/\theta^*)_{\text{proto}}$$

4. Heat rejection rate scaling:

$$\frac{\dot{Q}_{R(\text{model})}}{\dot{Q}_{R(\text{proto})}} = \frac{(h_{\text{conv}} A)_{\text{model}}}{(h_{\text{conv}} A)_{\text{proto}}}$$

where  $A$  is  $2\pi r_0 L$ .

### Development of the scaling relationships

Extrapolation to the prototype may be accomplished by plotting  $T_{\text{in}}$  and  $T_{\text{out}}$  vs  $(\theta/\theta^*)$  and  $(r/r_0)$  vs  $(\theta/\theta^*)$ ; these relationships are applicable for a specific  $\Delta T(T_{\text{in}} - T_{\text{out}})$  condition. The time scale is established by selection of the flow rate ( $W/M$ ):

$$\theta^* = \frac{M_{\text{sink}}}{W} \frac{(H + C_p T_{\max})}{C_p \Delta T} = \frac{M_{\text{sink}}(H + C_p T_{\max})}{\dot{Q}_R}.$$

Thus

$$\frac{\theta^*_{\text{(model)}}}{\theta^*_{\text{(proto)}}} = \frac{\left( \frac{M_{\text{sink}}}{\dot{Q}_R} \right)_{\text{model}} (H + C_p T_{\max})}{\left( \frac{M_{\text{sink}}}{\dot{Q}_R} \right)_{\text{proto}} (H + C_p T_{\max})}.$$

Now

$$(H + C_p T_{\max})_{\text{model}} = (H + C_p T_{\max})_{\text{proto}}$$

so

$$\begin{aligned} \frac{\theta^*_{\text{model}}}{\theta^*_{\text{proto}}} &= \frac{(\rho_i \pi R_0^2 L / \dot{Q}_R)_{\text{model}}}{(\rho_i \pi R_0^2 L / \dot{Q}_R)_{\text{proto}}} \\ &= \frac{(R_0^2 L)_{\text{model}}}{(R_0^2 L)_{\text{proto}}} \frac{\dot{Q}_{R(\text{proto})}}{\dot{Q}_{R(\text{model})}} \end{aligned}$$

since

$$\frac{\dot{Q}_{R(\text{proto})}}{\dot{Q}_{R(\text{model})}} = \frac{(h_{\text{conv}} A)_{\text{proto}}}{(h_{\text{conv}} A)_{\text{model}}} = \frac{(h_{\text{conv}} 2 \pi r_0 L)_{\text{proto}}}{(h_{\text{conv}} 2 \pi r_0 L)_{\text{model}}}$$

The following relationship holds between model and prototype for the initial sink radius, relative to the total useful sink life:

$$\begin{aligned} \frac{\theta^*_{\text{model}}}{\theta^*_{\text{proto}}} &= \frac{(r_0^2 L)_{\text{model}}}{(r_0^2 L)_{\text{proto}}} = \frac{(h_{\text{conv}} r_0 L)_{\text{proto}}}{(h_{\text{conv}} r_0 L)_{\text{model}}} \\ &= \frac{r_0(\text{model})}{r_0(\text{proto})} \frac{h_{\text{conv}}(\text{proto})}{h_{\text{conv}}(\text{model})}. \quad (\text{B8}) \end{aligned}$$

As noted previously for turbulent flow,  $h_{\text{conv}}$  is independent of size; thus

$$h_{\text{conv}(\text{proto})} = h_{\text{conv}(\text{model})}$$

It should be recognized that for a scale-model test experiencing laminar flow, any extrapolation to a large size sink undergoing turbulent heat transfer will result in conservative estimates of coolant water heating rates. Turbulent flow will induce greater mixing and will thus produce higher heat transfer coefficients (higher Nusselt numbers). Consequently, experimental results obtained under laminar flow will,

when extrapolated to a large sink, tend to err on the conservative side under the similarity relations derived above.

Thus

$$\frac{\theta^*_{\text{model}}}{\theta^*_{\text{proto}}} = \frac{R_0(\text{model})}{R_0(\text{proto})}$$

and

$$\dot{Q}_{R(\text{proto})} = \frac{(R_0 L)_{\text{proto}}}{(R_0 L)_{\text{model}}} \dot{Q}_{R(\text{model})}$$

also

$$\left( \frac{W \theta^*}{M_{\text{sink}} \text{model}} \right) = \left( \frac{W \theta^*}{M_{\text{sink}} \text{proto}} \right)$$

$$W_{\text{proto}} = \left( \frac{\theta^*}{M_{\text{sink}} \text{model}} \right) \left( \frac{M_{\text{sink}}}{\theta^*} \right)_{\text{proto}} W_{\text{model}}$$

$$= \left( \frac{R_0}{M_{\text{sink}} \text{model}} \right) \left( \frac{M_{\text{sink}}}{R_0} \right)_{\text{proto}} W_{\text{model}}$$

$$= \left( \frac{R_0}{\pi R_0^2 L \text{model}} \right) \frac{\pi R_0^2 L}{R_0} W_{\text{model}}$$

$$= \frac{(R_0 L)_{\text{proto}}}{(R_0 L)_{\text{model}}} W_{\text{model}} \quad (\text{B9})$$

Using the above relationships, the dimensional and heat transfer similarities are satisfied. For the series of experiments conducted during the study of the ice water heat sink concept, Table AI provides a comparison between the scale models and the prototype based on nominal tank dimensions.

Table AI. Comparison between the scale models and the prototype based on nominal tank dimensions.

	Prototype sink (6.5 ft diam $\times$ 110 ft)	Model II sink (6 ft diam $\times$ 10 ft)	Model I sink (4 ft diam $\times$ 6 ft)
Heat rejection rate (Btu/hr)	5.96 $\times 10^6$ 5.22 $\times 10^6$ 2.61 $\times 10^6$	47,763* 42,013 21,006*	19,105 16,805 8,405
Coolant water flow rate (gpm)	1,680 1,245 935 590 310 205	13.50 10.00 7.50 4.73 2.50 1.55*	5.40 4.00 3.00 1.89 1.00 0.62

\* No tests were conducted at this value.

## APPENDIX C: DERIVATION OF THE RELATIONSHIPS FOR THE HEAT TRANSFER COEFFICIENT, REYNOLDS AND NUSSELT NUMBERS

Relationships are developed here to approximate the heat transfer coefficient, Reynolds number and Nusselt number. Sample calculations are also included to illustrate the application of these relationships.

### Heat transfer coefficient

A first order approximation of the coefficient of heat transfer can be made by considering the gross melting process which occurs within the heat sink. Considering only that portion of the total heat rejected to the ice  $dQ_m$  during any finite period of time, we have

$$dQ_m = hA \Delta T_m dt$$

where  $h$  = heat transfer coefficient

$A$  = area of the melting surface

$\Delta T_m$  = temperature difference between the melting surface and the bulk water temperature

$dt$  = length of the time period.

If the ice is initially at 32°F then all the heat rejected must be used to melt the ice. If it is assumed that only radial melting occurs and melting is uniform along the height of the ice cylinder, then

$$dQ_m = L dM_i$$

where  $M_i = \rho_i \pi R^2 H$ . Therefore

$$dQ_m = \rho_i L 2\pi R H dR$$

where  $\rho_i$  = density of the ice

$L$  = latent heat of fusion

$R$  = radius of the ice cylinder

$H$  = height of the ice cylinder (constant).

Since melting is assumed to occur only on the circumferential surface of the ice, the factor of  $2\pi RH$  is the effective melting surface area. Therefore the equation becomes

$$dQ_m = \rho_i L A dR$$

From this expression and the relation involving the heat transfer coefficient, the following expression is obtained:

$$h = \frac{\rho_i L}{\Delta T_m} \frac{dR}{dt} \quad (C1)$$

Thus, the heat transfer coefficient can be approximated when the rate of radial melting and the bulk water temperature are known. Since both these parameters vary with time and elevation in the sink, a specific determination of the heat transfer coefficient is not possible.

To approximate the heat transfer coefficient it can be assumed, as a first order approximation, that the bulk water temperature would be equal to the average value of the inlet and outlet water during the melting period. That is

$$T_B = \frac{1}{2} (\bar{T}_{in} + \bar{T}_{out}) \quad (C2)$$

where  $\bar{T}_B$  = average bulk water temperature during melting

$\bar{T}_{in}$  = average inlet water temperature during melting

$\bar{T}_{out}$  = average outlet water temperature during melting.

From this the mean temperature difference between the ice and the water  $\Delta T_m$  is

$$\Delta T_m = \bar{T}_B - 32. \quad (C3)$$

Considering the melting process with respect to a time interval of duration  $\Delta t$  hours the rate of change in radius can be approximated by

$$\frac{dR}{dt} \approx \frac{\Delta R}{\Delta t}$$

where  $\Delta R$  is the change in the radius during the time interval  $\Delta t$ . Thus the approximation for the heat coefficient becomes

$$h = \frac{\rho_i L}{\left[ \frac{1}{2}(T_{in} + T_{out}) - 32 \right]} \frac{\Delta R}{\Delta t} \quad (C4)$$

The application of this equation is not restricted to any specific time interval duration. If  $\Delta t$  is selected to be the total melting period, then  $\Delta R$  would be the change in radius from the initial value to zero. If  $\Delta t$  is less than the total melting period, the change in the radius for that period must be approximated using additional information, such as the rate of melting.

#### Reynolds number

Nondimensional parameters have been employed to establish a generalized correlation between the heat transfer coefficient and the coolant water flow rates. Water velocity effects are normally considered by use of a Reynolds number  $Re$  where

$$Re_D = \frac{UD}{v}$$

where  $U$  = mean water velocity (ft/hr)

$D$  = characteristic dimension (diameter) (ft)

$v$  = kinematic viscosity (ft<sup>2</sup>/hr).

For flow in annular passages the characteristic dimension normally selected is the "equivalent" diameter of the annulus<sup>4</sup> which is defined by

$$DE = \frac{4 \frac{\pi}{4} (D_2^2 - D_1^2)}{\pi(D_2 + D_1)} = (D_2 - D_1) \quad (C5)$$

where  $DE$  = equivalent diameter (ft)

$D_2$  = outer diameter of the annulus (ft)

$D_1$  = inner diameter of the annulus (ft).

In the ice-water heat sink,  $D_2$  is the diameter of the test apparatus (constant) while  $D_1$  is the average diameter of the ice cylinder during the interval of approximation (variable). The mean water velocity is determined by dividing the volumetric flow rate by the average cross-sectional area of the annulus. Thus, the mean flow velocity is calculated from

$$U = \frac{\frac{W}{\rho_w}}{\frac{\pi(D_2^2 - D_1^2)}{4}} \quad (C6)$$

where  $W$  = mass flow rate (lbm/hr) and  $\rho_w$  = density of water (lbm/ft<sup>3</sup>).

Substituting these equations into the expression for the Reynolds number yields

$$Re_{DE} = \frac{4W}{\pi\rho_w v(D_t + D_i)} \quad (C7)$$

where  $D_t$  is nominal tank diameter (ft), and  $D_i$  is the average ice diameter during the time interval of approximation.

The Reynolds number is approximated for the same series of time intervals as the heat transfer coefficient.

#### Nusselt number

The Nusselt number is employed to nondimensionalize the heat transfer coefficient for correlation with the Reynolds number. This relationship is

$$Nu_q = \frac{hH_0}{k} \quad (C8)$$

where  $h$  = heat transfer coefficient (Btu/hr ft<sup>2</sup> °F)

$H_0$  = initial height of the ice cylinder (ft)

$k$  = thermal conductivity of the water (Btu/hr ft °F).

The use of the initial ice cylinder height as the characteristic dimension agrees with the assumptions employed in the approximation of the heat transfer coefficient and appears to provide a reasonable correlation. The basis for this selection was discussed previously.

#### Sample calculation

To illustrate the application of these relationships, the heat transfer coefficient, Reynolds and Nusselt numbers for the first 10-hour interval of test 1B will be calculated. The data used in these sample calculations can be found in Table II.

*Heat transfer coefficient.* From equation C4

$$h = \frac{\rho_i L}{\left[ \frac{1}{2}(T_{in} + T_{out}) - 32 \right]} \frac{\Delta R}{\Delta t} \quad$$

Using the constants

$$\rho_i = 56.7 \text{ lbm/ft}^3$$

$$L = 144 \text{ Btu/lbm}$$

and the following data for the first 10 hours of test 1B

$$\bar{T}_{in} = 54.2^\circ\text{F}$$

$$\bar{T}_{out} = 37.7^\circ\text{F}$$

$$\Delta R = 0.34 \text{ ft}$$

$$\Delta t = 10 \text{ hr}$$

$$h = \frac{(56.7)(144)}{\left[\frac{1}{2}(54.2+37.7)-32\right]} \frac{0.34}{10} \text{ Btu/hr ft}^2 \text{ }^\circ\text{F}$$

algebraic average of the bulk water temperature and the temperature of the heat transfer surface (i.e., the ice). For this example the mean fluid temperature  $T_f$  is

$$T_f = \frac{1}{2}(46.0+32.0)^\circ\text{F} = 39^\circ\text{F}.$$

The thermal conductivity is evaluated at  $39^\circ\text{F}$ , so that the Nusselt number is

$$Nu_g = \frac{(19.90 \text{ Btu/hr ft}^2 \text{ }^\circ\text{F})(8.68 \text{ ft})}{(0.331 \text{ Btu/hr ft}^2 \text{ }^\circ\text{F})}$$

or

$$Nu_g = 522.$$

or

$$h = 19.90 \text{ Btu/hr ft}^2 \text{ }^\circ\text{F}.$$

*Reynolds number.* The nominal test flow rate was 4.73 gpm or  $37.94 \text{ ft}^3/\text{hr}$ . During the first 10 hours the ice radius changes from 3.00 ft to 2.66 ft ( $\Delta R = 0.34 \text{ ft}$ ) so that the average ice radius is 2.83 ft. The kinematic viscosity is evaluated at the bulk water temperature of  $46.0^\circ\text{F}$ ; thus, the following constants apply:

$$W = 37.94 \rho_w \text{ (lbm/hr)}$$

$$D_t = 6.00 \text{ (ft)}$$

$$D_i = \frac{1}{2}(6.00+5.32) = 5.66 \text{ (ft)}$$

$$v = 0.0545 \text{ (ft}^2/\text{hr}).$$

Thus from eq C7

$$Re_{DE} = \frac{(4)(37.94 \rho_w)}{\pi \rho_w (0.0545)(6.00+5.66)}$$

$$Re_{DE} = 76.0.$$

*Nusselt number.* The height employed in eq C8 is 8.68 ft and the thermal conductivity of the water is evaluated at the mean fluid temperature, which is the

## APPENDIX D: DETERMINATION OF FREEZING RATES AND REFRIGERATION LOADS\*

The freezing geometry of the heat sink is illustrated in Figure D1. The use of the cooling coils along the tank wall results in radial freezing inward from the wall. Freezing at the bottom of the tank and end effects at the upper surface have been neglected in order to develop a simplified prediction technique. The water in the tank is assumed to be initially at 32°F.

With these assumptions the freezing of the sink is dependent only upon the radial coordinate, and thus the temperature distribution in the ice annulus is governed by the following partial differential equation:

$$\rho c_p \frac{\partial T}{\partial t} - k \frac{\partial}{\partial R} \left( R \frac{\partial T}{\partial R} \right) = 0.$$

The associated boundary conditions are

$$T(R_0, t) = T_0$$

$$T(R_m, t) = T_1 = 32^\circ\text{F}$$

where  $R_m$  = radius at ice/water interface. The heat transfer at the ice/water interface is described by the following relationship:

$$\frac{\partial R}{\partial t} = \frac{k}{\rho_i L} \frac{\partial T}{\partial R} \Big|_{R=R_m}$$

Since the variation in ice temperature with time is slow, a steady state solution to the differential equation may be used. Thus the temperature at any time  $t$  is given by

$$T(t) = T_0 + \frac{(T_1 - T_0) \ln \left( \frac{R_0}{R} \right)}{\ln \left( \frac{R_0}{R_m(t)} \right)} \quad (\text{D1})$$

Upon substitution of this relationship into the heat transfer relationship, the following expression for the time required to form an ice annulus of radius  $R_m$  results:

$$t = \frac{\rho_i L R_0^2}{4k(T_1 - T_0)} \left\{ 1 - \left( \frac{R_m}{R_0} \right)^2 \left[ 1 - 2 \ln \left( \frac{R_m}{R_0} \right) \right] \right\} \quad (\text{D2})$$

\* Original derivation of equations by E. Grande, reference 7.

For the Model II heat sink the following are the parameter values to be employed:

$$R_0 = 3.0 \text{ ft}$$

$$\rho_i = 56.7 \text{ lbm/ft}^3$$

$$L = 144 \text{ Btu/lbm}$$

$$T_1 = -70^\circ\text{F}$$

$$k = 1.26 \text{ Btu/hr ft } ^\circ\text{F.}$$

These values were substituted into the above equation and Figure D2 was developed to show the rate of growth of the ice annulus with time. This relationship predicts that freezing of the Model II sink will occur within 6 days, which agrees with the measured freeze-up time. Although the tank wall temperature was not -70°F at the start of freezing, only 3 to 4 hours was required to attain that temperature.

It should also be noted that the water within the tank was agitated by the air bubbling system and that, although the equation used to estimate freezing times is for freezing along a quiescent boundary, it predicted the overall freezing time rather well.

An estimation of the rate of heat flow to the refrigeration coils can be made from

$$\dot{Q} = 2\pi R_0 H_0 k \frac{\partial T}{\partial R} \Big|_{R=R_m}$$

which upon substitution of the expression for  $T$  becomes

$$\dot{Q} = \frac{2\pi H_0 k (T_1 - T_0)}{\ln \left( \frac{R_0}{R_m} \right)}$$

Using a value of  $H_0 = 9.0 \text{ ft}$  (a typical test dimension) the variation in heat flow with respect to time has also been plotted in Figure D2. After the first day the rate of heat flow has decreased from more than 68,000 Btu/hr to approximately 20,000 Btu/hr as a result of formation of a 1-ft-thick annular section of ice.

It had been originally assumed that the length of the freezing period could be substantially reduced by preloading the sink with ice blocks; however, a more detailed examination tended to conflict with this line of reasoning. An examination of Figure D3, which shows the theoretical rate of freezing based on volume, indicated that 51% of the mass of the Model II sink was already frozen at the end of the first day. It should be noted that when the sink was preloaded with approximately 50% ice, the length of the freezing period was reduced by only one day. Thus, the observed decrease correlates well with the predicted behavior, even though two "distinct" sets of freezing conditions exist. Further examination of Figure D3 indicates why both of these zones agree. Note that during the last day of freezing only 3% of the total volume becomes frozen; during the last two days only 10% of the total volume can be frozen, even though a wall temperature of  $-70^{\circ}$  is used. This is a result of the long path through which the heat must be conducted, which during the last two days varies

from 2.1 to 3.0 ft at the completion of freezing. Independent of whether or not the outer layer was composed of ice blocks or frozen water, the length of this path remains the same. Thus a substantial decrease in the length of the freezing period is possible only if the length of the heat conduction path is made shorter or a massive initial ice load is used. To decrease the freezeup period by 50%, it would be necessary to have an initial load of ice equal to 82% of the total mass of the sink. It should be noted that in previous solid cylinder tests the percentage of ice mass was on the order of 85% to 90% of total mass, and thus preloading blocks to achieve an 82% load factor would be impossible.

This is not to say that preloading with ice is without benefit. In Figure D2 it can be seen that the greatest heat load on the refrigeration system occurs during the same period that the initial 50% of the sink mass is frozen. Thus preloading of ice can be translated into reduced initial heat loads and reduced refrigeration costs.

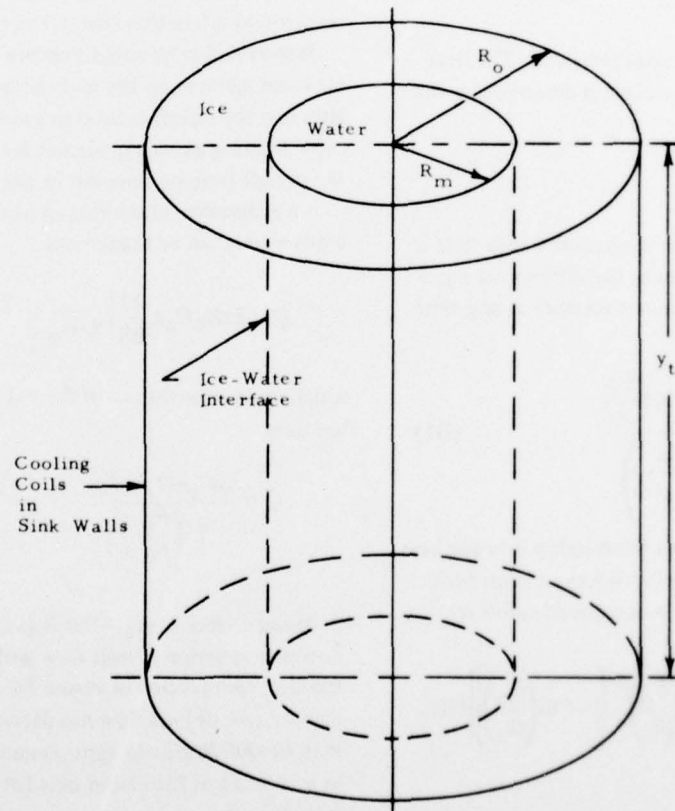


Figure D1. Freezing geometry of the heat sink.

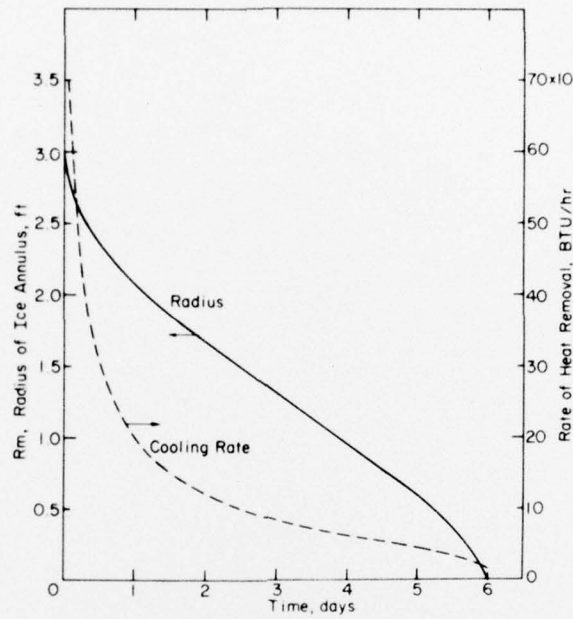


Figure D2. Growth of ice annulus during freezing.

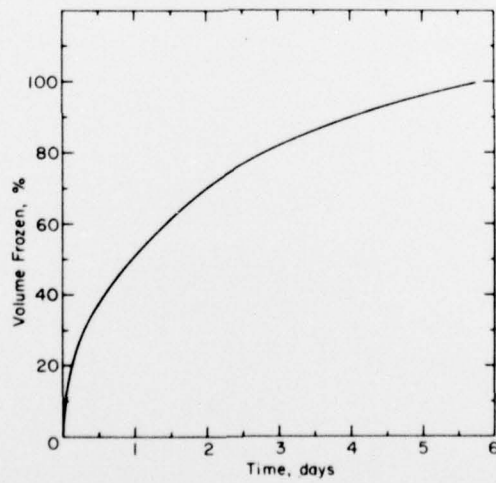


Figure D3. Volumetric freezing rate.

## APPENDIX E: APPROXIMATION OF STRESSES IN THE HEAT SINK TANK

In the previous ice-water heat sink study<sup>14</sup> it had been observed that fractures occurred in the ice after freezing had been completed and the heating cycle started. During assembly of the Model II tank, bonded strain gages were installed to monitor induced wall stresses during the thawing mode. However, because of damage during tank assembly only one measuring gage and the temperature compensating gage were operational during the test program. The temperature compensating gage was mounted on a section of steel of the same type as used to make the heat sink tank and exposed to the same temperature conditions as the tank wall. When connected in a bridge network with the measuring gage, the temperature compensating gage eliminates the apparent strain readings that result from temperature-induced expansion or contraction of the tank wall. The active gage was located at the midheight of the tank and was mounted in the circumferential direction to measure induced hoop stresses. A thermocouple mounted at the same location on the inside of the tank was used to measure tank wall temperature.

As an approximation of the true stress condition it can be assumed that the heat sink tank experiences a stress condition similar to that of a long, thin-walled pressure vessel without edge effects, subjected to a uniform internal pressure. Actually the Model II tank is a rather short vessel with a length to diameter ratio of only 1.33 to 1, but since the gages were mounted at midheight, this assumed stress condition represents a reasonable first-order approximation.

Under such a stress condition the stress in the wall can be expressed as

$$\sigma_{\theta} = \frac{PR}{t} \quad (E1)$$

where  $\sigma_{\theta}$  = circumferential wall stress (hoop stress)

$P$  = internal pressure

$R$  = radius of the cylinder (36.0 in.)

$t$  = wall thickness (0.375 in.).

Since from Hooke's law

$$\sigma_{\theta} = E \epsilon_{\theta}$$

where  $E$  is Young's modulus ( $30 \times 10^6$  lbf/in.<sup>2</sup> for steel) and  $\epsilon_{\theta}$  is hoop strain, then

$$P = \frac{Et}{R} \epsilon_{\theta} \quad (E2)$$

To establish a base value for strain measurements, a reading of the strain gages was taken with a water head of 9 ft and at a wall temperature of 44°F (simulated operation). Using the above relationship and the strain readings during the heating period just after the completion of freezing, the internal pressures as a function of tank wall temperature were calculated. The results are presented in Figure E1. Also shown is the variation in hoop stress in the tank wall.

The figure indicates that, as the tank wall temperature increases from -70°F to 20°F, there are significant variations in the internal pressure and thus the stress induced in the wall. As its temperature increases, the ice cylinder attempts to expand in volume; however, since the tank wall limits the total amount of volumetric expansion possible, significant stresses are induced in both the ice and tank wall. The sudden decreases in stress which are evident on Figure E1 most likely result from the propagation of cracks within the ice. Of course ice cracking is not restricted to the period following the initial heating of the ice; localized stress concentrations can produce cracks at any time during the heating process.

What is worth noting in this experiment is the magnitude of the induced stresses. The measurements indicate maximum, minimum, and average internal pressures of 100.4, 34.3, and 79.7 lb/in.<sup>2</sup>, respectively, and corresponding maximum, minimum and average hoop stresses of 10,200, 3,300 and 7,620 lb/in.<sup>2</sup>, respectively. Of course these stresses and pressures are functions of the experimental tank conditions, i.e., a 9-ft water head and an initial wall temperature of 44°F.

These observed wall stresses are significantly greater than the nominal unconfined fracture strength of ice. In general this indicates that, in the operation of a prototype, significant tank stresses

may be induced during the time that the ice is being initially heated to form the annular gap between the tank and ice cylinder walls.

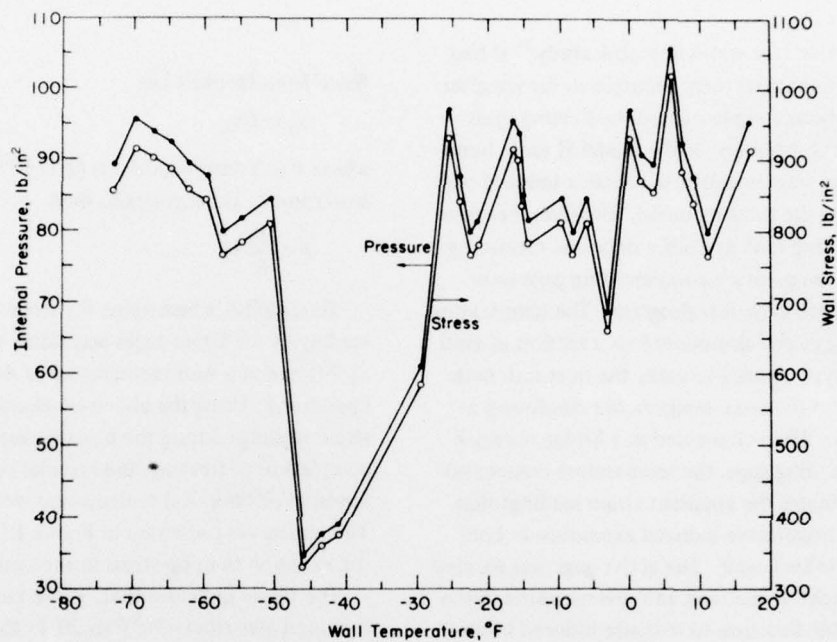


Figure E1. Variations in internal pressure and tank wall stress during the ice heating mode.